

## Iron(II) Complexes with Amide-Containing Macrocycles as Non-Heme Porphyrin Analogues

Ivan V. Korendovych,<sup>†</sup> Olga P. Kryatova,<sup>†</sup> William M. Reiff,<sup>\*‡</sup> and Elena V. Rybak-Akimova<sup>\*†</sup>

Department of Chemistry, Tufts University, Medford, Massachusetts 02155, and Department of Chemistry and Chemical Biology, Northeastern University, Boston, Massachusetts 02115

Received January 23, 2007

Iron(II) complexes of macrocyclic pentadentate ligands 3,6,9,12,18-pentaazabicyclo[12.3.1]octadeca-1(18),14,16-triene-2,13-dione ( $H_2pydioneN_5$ ) and 16-chloro-3,6,9,12,18-pentaazabicyclo[12.3.1]octadeca-1(18),14,16-triene-2,13-dione ( $H_2pyCldioneN_5$ ) were synthesized and fully characterized. Complexes with one or two deprotonated amide groups of  $H_2pydione$  were both isolated. In the former case the metal ion has a distorted octahedral coordination sphere; in the latter case the complex adopts a pentagonal–bipyramidal geometry. NMR experiments show that the protonation state of the ligand is preserved in a dimethyl sulfoxide (DMSO) solution. The complexes maintain a high-spin state even at low temperatures. Detailed kinetic studies of oxygenation of the iron(II) complexes showed that the deprotonation state of the complex has a profound effect on the reactivity with dioxygen. Oxygenation of the dideprotonated complex of iron(II),  $Fe(pydioneN_5)$ , in aprotic solvents proceeds via a path that is analogous to that of iron(II) porphyrins: via iron(III) superoxo and diiron(III) peroxy species, as evidenced by the spectral changes during the reaction, which is second-order in the concentration of the iron(II) complex, and with an inverse dependence of the reaction rate on the concentration of dioxygen. The final products of oxygenation are crystallographically characterized iron(III)  $\mu$ -oxo dimers. We have also found that the presence of 1-methylimidazole stabilizes the diiron peroxy intermediate. The reaction of  $Fe(pydioneN_5)$  with dioxygen in methanol is distinctly different under the same conditions. The reaction is first-order in both iron(II) complex and dioxygen, and no intermediate is spectroscopically observed. Similar behavior was observed for the monodeprotonated complex  $Fe(HpydioneN_5)(Cl)$ . The presence of an accessible proton either from the solvent (reactions in methanol) or from the complex itself (in  $Fe(HpydioneN_5)(Cl)$ ) proves sufficient to alter the oxygenation pathway in these macrocyclic systems, which is reminiscent of the properties of iron(II) porphyrin complexes. The new amidopyridine macrocycles can be considered as new members of the “expanded porphyrin analogue” family. The expansion of the cavity provides control over the spin state and availability of protons. These macrocyclic systems also allow for easy synthetic modifications, paving the way to new, versatile metal complexes.

### Introduction

Understanding the mechanisms of dioxygen activation at the metal centers is important for unraveling the mechanisms of metal-containing oxidases and oxygenases, and for synthesizing new selective oxidation catalysts. Nature has developed numerous metalloprotein systems that utilize dioxygen for the selective oxidation of various substrates. Iron-containing proteins, which are among the most common enzymes that are responsible for substrate ox-

idation, are generally subdivided into two general groups: heme and non-heme iron enzymes. The former group of metalloproteins has been extensively studied, and a great deal of understanding of their function has been achieved. Until recently, much less knowledge was available on the non-heme iron enzymes.<sup>1</sup> Understanding of these metalloproteins was greatly facilitated by the structural, spectroscopic, and mechanistic investigations of synthetic inorganic model complexes.<sup>1–6</sup>

\* To whom correspondence should be addressed. E-mail: w.reiff@neu.edu (W.M.R.), elena.rybak-akimova@tufts.edu (E.V.R.-A.).

<sup>†</sup> Tufts University.

<sup>‡</sup> Northeastern University.

(1) Costas, M.; Mehn, M. P.; Jensen, M. P.; Que, L., Jr. *Chem. Rev.* **2004**, *104*, 939–986.

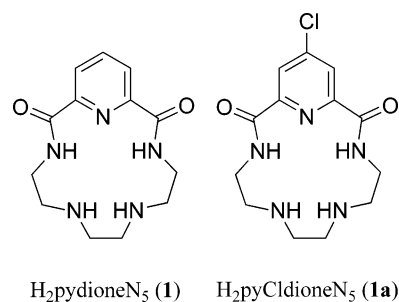
(2) Collman, J. P.; Boulatov, R.; Sunderland, C. J.; Fu, L. *Chem. Rev.* **2004**, *104*, 561–588.

Our approach to the design of functional models of natural systems is based on iron complexes with macrocyclic ligands. Macrocyclic ligands were chosen for their relative rigidity, which results in a predictable coordination geometry of the metal, and for their high thermodynamic and kinetic stability of complexes, which prevents uncontrolled metal leakage, oxidation, and hydrolysis. Macrocycles of variable size and number of donor atoms are readily accessible by synthetic means. Amide groups, which can be incorporated into the rings, are expected to stabilize the high oxidation state of the coordinated metal ion relative to its lower oxidation state(s), thus facilitating oxygen binding and activation at the iron center. Iron complexes with amide-containing ligands provide insight into the structure and function of important metalloproteins, such as iron bleomycin<sup>7–9</sup> and nitrile hydratase.<sup>10,11</sup> Such systems can also be catalytically active in oxidation reactions.<sup>12,13</sup>

We have recently shown that, unlike the majority of strongly  $\sigma$ -donating electron-rich amide-containing ligands that form low-spin complexes,<sup>14–23</sup> the pentaaza macrocyclic ligand 3,6,9,12,18-pentaazabicyclo[12.3.1]octadeca-1(18),14,16-triene-2,13-dione ( $H_2$ pydione $N_5$ , **1**) (Scheme 1) (which enforces pentagonal–bipyramidal geometry and thus precludes the low-spin state of  $d^5$  or  $d^6$  metal ions<sup>24</sup>) forms exclusively high-spin Fe(III) complexes, even in the presence of strong axial ligands.<sup>25</sup>

Controlling the spin state of iron is important for modulating the redox reactivity of iron complexes.<sup>26</sup> Therefore, such ligands that provide access to a predetermined spin state and

Scheme 1



geometry of the metal center are of particular interest for studies of oxygen and peroxide activation. The fairly large macrocyclic cavity of **1** also allows for the isolation of metal complexes with different numbers of amide groups coordinated to the iron atom. The non-coordinated, ionizable amide group can provide a proton immediately at the reaction center, and thus it enables us to study the effect of  $H^+$  on the oxygen activation pathways.

These properties are similar to those of porphyrins, but amide-containing macrocycles provide additional possibilities for controlling the electronic and steric structure of iron complexes. Development of these new ligands, which are easier to synthesize and modify, permits the expansion of the “standard” porphyrin chemistry while affording similar stability and chemical properties. The tuning of steric and electronic properties can also be achieved. In a sense, this new macrocyclic system can be considered a “non-pyrrole porphyrin analogue”. Recently, there have been numerous new developments in the design of “porphyrin analogues”. The interest is predominantly driven by three new possibilities: (1) the incorporation of more than one metal ion into the macrocyclic cavity, (2) the variation of coordination mode via design of more flexible macrocycles, (3) and pre-organization of the metal sites for catalysis and enzyme mimicking.<sup>27,28</sup> Progress in this field has resulted in the development of various porphyrin analogues that include expanded porphyrins,<sup>28</sup> corroles,<sup>29</sup> N-confused porphyrins,<sup>30</sup> and accordion porphyrins,<sup>31</sup> to name just a few. Reversible oxygen binding was observed for more distant relatives, such as iron and cobalt cyclidene complexes that were developed by Busch and co-workers.<sup>32</sup>

Significant progress has been achieved in the synthesis of Fe(III) complexes with various amide-containing ligands,<sup>33</sup> but the coordination chemistry of Fe(II) with similar systems, which are better suited for studies of oxygenation, is much less explored.<sup>23,34,35</sup> This paper describes the preparation of

- (3) Kovacs, J. *Chem. Rev.* **2004**, *104*, 825–848.
- (4) Kryatov, S. V.; Rybak-Akimova, E. V.; Schindler, S. *Chem. Rev.* **2005**, *105*, 2175–2226.
- (5) Walker, F. A. *Chem. Rev.* **2004**, *104*, 589–615.
- (6) Tsuva, E. Y.; Lippard, S. J. *Chem. Rev.* **2004**, *104*, 987–1012.
- (7) Burger, R. M. *Chem. Rev.* **1998**, *98*, 1153–1169.
- (8) Hecht, S. M. *Acc. Chem. Res.* **1986**, *19*, 383–391.
- (9) Stubbe, J.; Kozarich, J. W.; Wu, W.; Vanderwall, D. E. *Acc. Chem. Res.* **1996**, *29*, 322–330.
- (10) Huang, W.; Jia, J.; Cummings, J.; Nelson, M.; Schneider, G.; Lindqvist, Y. *Structure* **1997**, *5*, 691–699.
- (11) Nagashima, S.; Nakasako, M.; Dohmae, N.; Tsujimura, M.; Takio, K.; Odaka, M.; Yohda, M.; Kamiya, N.; Endo, I. *Nat. Struct. Biol.* **1998**, *5*, 347–351.
- (12) Collins, T. J. *Acc. Chem. Res.* **1994**, *27*, 279–285.
- (13) Nguen, C.; Guajardo, R. J.; Mascharak, P. K. *Inorg. Chem.* **1996**, *35*.
- (14) Ray, M.; Ghosh, D.; Shirin, Z.; Mukherjee, R. *Inorg. Chem.* **1997**, *36*, 3568–3572.
- (15) Tao, X.; Stephan, D. W.; Mascharak, P. K. *Inorg. Chem.* **1987**, *26*, 754–759.
- (16) Noveron, J. C.; Olmstead, M. M.; Mascharak, P. K. *Inorg. Chem.* **1998**, *37*, 1138–1139.
- (17) Harrop, T. C.; Tyler, L. A.; Olmstead, M. M.; Mascharak, P. K. *Eur. J. Inorg. Chem.* **2003**, 475–481.
- (18) Marlin, D. S.; Olmstead, M. M.; Mascharak, P. K. *Inorg. Chem.* **1999**, *38*, 3258–3260.
- (19) Marlin, D. S.; Olmstead, M. M.; Mascharak, P. K. *Eur. J. Inorg. Chem.* **2002**, 859–865.
- (20) Rowland, J. M.; Olmstead, M. M.; Mascharak, P. K. *Inorg. Chem.* **2001**, *40*, 2810–2817.
- (21) Che, C.-M.; Leung, W.-H.; Li, C.-K.; Cheng, H.-Y.; Peng, S.-M. *Inorg. Chim. Acta* **1992**, *196*, 43–48.
- (22) Guajardo, R. J.; Hudson, S. E.; Brown, S. J.; Mascharak, P. K. *J. Am. Chem. Soc.* **1993**, *115*, 7971–7977.
- (23) Brown, S. J.; Olmstead, M. M.; Mascharak, P. K. *Inorg. Chem.* **1990**, *29*, 3229–3234.
- (24) Hoffmann, R.; Beier, B. F.; Muetterties, E. L.; Rossi, A. R. *Inorg. Chem.* **1977**, *16*, 511–522.
- (25) Korendovych, I. V.; Staples, R. J.; Reiff, W. M.; Rybak-Akimova, E. V. *Inorg. Chem.* **2004**, *43*, 3930–3941.

- (26) Fujita, M.; Costas, M.; Que, L., Jr. *J. Am. Chem. Soc.* **2003**, *125*, 9912–9913.
- (27) Sessler, J. L.; Tomat, E.; Mody, T. D.; Lynch, V. M.; Veauthier, J. M.; Mirsaidov, U.; Markert, J. T. *Inorg. Chem.* **2005**, *44*, 2125–2127.
- (28) Sessler, J. L.; Seidel, S. *Angew. Chem., Int. Ed.* **2003**, *42*, 5134–5175.
- (29) Gross, Z. J. *Biol. Inorg. Chem.* **2001**, *6*, 733–738.
- (30) Maeda, H.; Furuta, H. *Pure Appl. Chem.* **2006**, *78*, 29–44.
- (31) Reiter, W. A.; Gerges, A.; Lee, S.; Deffo, T.; Clifford, T.; Danby, A.; Bowman-James, K. *Coord. Chem. Rev.* **1998**, *174*, 343–359.
- (32) Busch, D. H.; Alcock, N. W. *Chem. Rev.* **1994**, *94*, 585–623.
- (33) Marlin, D. S.; Mascharak, P. K. *Chem. Soc. Rev.* **2000**, *29*, 69–74.
- (34) Umezawa, H.; Takita, T.; Yukio, S.; Masami, O.; Kobayashi, S.; Ohno, M. *Tetrahedron* **1984**, *40*, 501–509.

mono- and dideprotonated iron(II) complexes of **1** and 16-chloro-3,6,9,12,18-pentaazabicyclo[12.3.1]octadeca-1(18),-14,16-triene-2,13-dione (H<sub>2</sub>pyCldioneN<sub>5</sub>, **1a**), their structural and spectroscopic characterization, and detailed studies of their reactivity with dioxygen. We have observed a profound effect of H<sup>+</sup> (either provided by the solvent or present in the ligand itself) on the oxygenation pathway.

## Experimental Section

**General.** NMR spectra were recorded on a Bruker DPX-300 spectrometer. UV-Vis spectra were recorded over the 200–1100 nm range on a Jasco V-570 spectrometer. Variable temperature UV-vis studies were performed with a PC2000 CCD array spectrometer equipped with a TP300-UV-VIS Transfection Dip Probe (Ocean Optics Inc.) over the 350–800 nm range using a modified setup as described by Rivera et al.<sup>36</sup> (Figure S1, Supporting information) IR spectra were recorded in KBr pellets on a Mattson 1000 Fourier transform IR (FT-IR) spectrometer at a 2 cm<sup>-1</sup> resolution. Electrospray (ESI) mass spectrometry was performed on a Finnigan LTQ instrument. X-band electron paramagnetic resonance (EPR) spectra were recorded on a Bruker EMX spectrometer. Elemental analysis was performed at Schwarzkopf Microanalytical Laboratory (Woodside, NY).

**Materials.** All materials used were ACS reagent grade or better and were used without additional purification. 2,6-Pyridinedicarboxylic acid and anhydrous dimethylsulfoxide (DMSO) were purchased from Acros. All other reagents were purchased from Aldrich. 1,4,7,10-Tetraazadecane was dried over KOH at 60 °C and distilled over sodium prior to use. Iron(II) triflate,<sup>37,38</sup> ligand **1**,<sup>25</sup> and 4-chloro-2,6-dimethylpyridinedicarboxylate<sup>39</sup> were obtained according to publishing to published procedures.

**Synthesis of 1a.** A solution of 1.69 g (7.4 mmol) of 4-chloro-2,6-dimethylpyridinedicarboxylate in 150 mL of hot, dry methanol was prepared. While the solution was mixed vigorously, a second solution of 1.08 g (7.4 mmol) of 1,4,7,10-tetraazadecane dissolved in 25 mL of dry methanol was quickly added. The reaction mixture was heated under reflux for 24 h. The solvent was then removed in vacuo to yield a white solid residue, which was purified by column chromatography on silica (eluted with 5% CHCl<sub>3</sub> in MeOH, R<sub>f</sub> = 0.41) to produce 0.62 g (27%) of **1a**. <sup>1</sup>H NMR (300 MHz, CDCl<sub>3</sub>) δ 9.13 (t, J = 5.9 Hz, 2H, -C(O)NH-), 8.18 (s, 2H, β-H of the pyridine ring), 3.50 (q, J = 5.3 Hz, 4H, -C(O)NHCH<sub>2</sub>-), 2.96 (t, J = 5.6 Hz, 4H, -C(O)NHCH<sub>2</sub>CH<sub>2</sub>-), 2.85 (s, 4H, -CH<sub>2</sub>-NHCH<sub>2</sub>CH<sub>2</sub>NHCH<sub>2</sub>-), 1.1 (br, 2H, -CH<sub>2</sub>NHCH<sub>2</sub>-). <sup>13</sup>C NMR (75 MHz, CDCl<sub>3</sub>) δ 161.9 (2C), 150.1 (2C), 147.9 (1C), 124.2 (2C), 49.9 (2C), 47.6 (2C), 39.1 (2C). MS (ESI): 312.2 (100%, [M + H]<sup>+</sup>), 314.2 (33%, [M + 2 + H]<sup>+</sup>).

**Synthesis of Fe(HpydioneN<sub>5</sub>)(Cl)(MeOH).** In a glove box, a solution of 199 mg (1 mmol) of iron(II) chloride tetrahydrate in 3 mL of dry methanol was slowly added to a vigorously stirred solution of 277 mg (2 mmol) of **1** in 5 mL of dry methanol to yield an intensely colored, purple solution of Fe(HpydioneN<sub>5</sub>)(Cl)(MeOH). In several days, 110 mg (Yield: 28%) of analytically

pure complex precipitated as dark-purple blocks. UV-vis (DMSO), λ<sub>max</sub>, nm (ε, M<sup>-1</sup>·cm<sup>-1</sup>): 574(550). Selected FT-IR absorption bands (KBr pellet, ν/cm<sup>-1</sup>): 3290–3190 (m, ν N–H); 3069, 2960–2805 (m, ν C–H); 1678 (vs, ν C=O non-coordinated); 1614 (vs, ν C=O coordinated); 1587 (s, ν<sub>pyridine ring</sub>); 1562 (s, ν C–N coordinated); 1537 (s, ν C–N non-coordinated). Anal. Calcd for C<sub>14</sub>H<sub>22</sub>-ClFeN<sub>5</sub>O<sub>3</sub>: C, 42.07; H, 5.55; N, 17.52. Found: C, 42.14; H, 5.51; N, 17.37.

**Synthesis of Fe(pydioneN<sub>5</sub>)(MeOH)<sub>2</sub>.** In a glove box, a solution of 871 mg (2 mmol) of iron(II) triflate in 3 mL of dry methanol was slowly added to a vigorously stirred solution of 554 mg (2 mmol) of **1** in 5 mL of dry methanol. The subsequent addition of 1 mL (7 mmol) of triethylamine yielded an intensely colored, purple solution of Fe(pydioneN<sub>5</sub>)(MeOH)<sub>2</sub>. In a few days, 550 mg (Yield: 69%) of the complex precipitated as dark-purple needles that could be washed with acetonitrile and were additionally purified by recrystallization from methanol. An additional crop of the material can be obtained by precipitation via ether diffusion. UV-vis (DMSO), λ<sub>max</sub>, nm (ε, M<sup>-1</sup>·cm<sup>-1</sup>): 602(1200). Selected FT-IR absorption bands (KBr pellet, ν/cm<sup>-1</sup>): 3280–3150 (m, ν N–H); 3060, 2950–2815 (m, ν C–H); 1612 (vs, ν C=O); 1589 (s, ν<sub>pyridine ring</sub>); 1570 (s, ν C–N). Anal. Calcd for C<sub>16</sub>H<sub>26</sub>FeN<sub>5</sub>O<sub>5</sub> (the formula refers to a trimethanol solvate which is in agreement with X-ray diffraction studies): C, 44.98; H, 6.84; N, 16.39; Fe, 13.07. Found: C, 45.57; H, 6.36; N, 17.72; Fe, 13.56. However, the elemental analysis better fits the formula of a dimethanol solvate (Anal. Calcd for C<sub>15</sub>H<sub>25</sub>FeN<sub>5</sub>O<sub>4</sub>: C, 45.58; H, 6.38; N, 17.72; Fe, 14.13). We attribute the difference to the loss, over time, of one loosely associated methanol molecule present in the crystal.

**Synthesis of [Fe(pyCldioneN<sub>5</sub>)(MeOH)<sub>2</sub>].** In a glove box, a solution of 435 mg (1 mmol) of iron(II) triflate in 3 mL of dry methanol was slowly added to a vigorously stirred solution of 312 mg (1 mmol) of **1a** in 5 mL of dry methanol. The subsequent addition of 0.75 mL (5 mmol) of triethylamine yielded an intensely colored, purple solution of Fe(pyCldioneN<sub>5</sub>)(MeOH)<sub>2</sub>. After several days, dark-blue plate like crystals precipitated. An additional amount of the complex can be obtained by the slow diffusion of ether in the methanol solution. Yield: 215 mg (46%). A different polymorph, Fe(pyCldioneN<sub>5</sub>)(MeOH), is obtained by the slow evaporation of methanol from concentrated solutions. UV-vis (DMSO), λ<sub>max</sub>, nm (ε, M<sup>-1</sup>·cm<sup>-1</sup>): 645 (1250). Selected FT-IR absorption bands (KBr pellet, ν/cm<sup>-1</sup>): 1611 (vs, ν C=O); 1593 (s, ν<sub>pyridine ring</sub>); 1573 (s, ν C–N). Anal. Calcd for C<sub>16</sub>H<sub>26</sub>ClFeN<sub>5</sub>O<sub>5</sub> (the formula refers to a trimethanol solvate in agreement with X-ray diffraction studies): C, 41.93; H, 5.63; N, 16.30; Fe, 13.00. Found: C, 42.30; H, 5.26; N, 16.44; Fe, 12.78.

**Isolation of Iron(III) μ-Oxo Dimers.** The compound [Fe(pyCldioneN<sub>5</sub>)(DMSO)]<sub>2</sub>O was obtained by the slow diffusion of air into a septum covered test tube, which contained 65 mg of Fe(pyCldioneN<sub>5</sub>)(MeOH)<sub>2</sub> dissolved in 4 mL of DMSO. The slow diffusion of air is essential for the formation of a crystalline solid. In a week, 25 mg of [Fe(pyCldioneN<sub>5</sub>)(DMSO)]<sub>2</sub>O was formed, and the product was collected by filtration and air-dried. Anal. Calcd for C<sub>30</sub>H<sub>60</sub>Cl<sub>2</sub>Fe<sub>2</sub>N<sub>10</sub>O<sub>15</sub>S<sub>2</sub> (the formula refers to [Fe(pydioneN<sub>5</sub>)(DMSO)]<sub>2</sub>O·8H<sub>2</sub>O): C, 34.40; H, 5.77; N, 13.37. Found: C, 34.17; H, 5.97; N, 13.70. A similar procedure was employed for the preparation of [Fe(pydioneN<sub>5</sub>)(1-MeIm)]<sub>2</sub>O; the slow diffusion of oxygen into solutions of Fe(pyCldioneN<sub>5</sub>)(MeOH)<sub>2</sub> (0.5–5 mM) in acetonitrile that contain 1-methylimidazole, (1–20% v/v) yields a microcrystalline precipitate of [Fe(pydioneN<sub>5</sub>)(1-MeIm)]<sub>2</sub>O. Anal. Calcd for C<sub>34</sub>H<sub>60</sub>Fe<sub>2</sub>N<sub>14</sub>O<sub>12</sub> (the formula refers to [Fe(pydioneN<sub>5</sub>)(1-MeIm)]<sub>2</sub>O·7H<sub>2</sub>O): C, 42.96; H, 6.24; N, 20.24. Found: C, 42.12; H, 6.18; N, 19.99. The analytical data in both cases seem to point

(35) Zhu, S.; Brennessel, W. W.; Harrison, R. G.; Que, L., Jr. *Inorg. Chim. Acta* **2002**, *337*, 32–38.

(36) Rivera, M.; Caignan, G. A.; Astashkin, A. V.; Raitsimring, A. M.; Shokhireva, T. K.; Walker, F. A. *J. Am. Chem. Soc.* **2002**, *124*, 6077–6089.

(37) Hagen, K. S. *Inorg. Chem.* **2000**, *39*, 5867–5869.

(38) Costas, M.; Que, L., Jr. (University of Minnesota). Personal communication (2002).

(39) Lamture, J. B.; Zhou, Z. H.; Kumar, A. S.; Wensel, T. G. *Inorg. Chem.* **1995**, *34*, 864–869.

**Table 1.** Crystallographic Data for Synthesized Complexes

chemical formula	C <sub>16</sub> H <sub>29</sub> FeN <sub>5</sub> O <sub>5</sub> [Fe(pydioneN <sub>5</sub> ) (MeOH) <sub>2</sub> ]·MeOH	C <sub>14</sub> H <sub>20</sub> ClFeN <sub>5</sub> O <sub>3</sub> [Fe(pyCldioneN <sub>5</sub> ) (MeOH)]	C <sub>16</sub> H <sub>28</sub> ClFeN <sub>5</sub> O <sub>5</sub> [Fe(pyCldioneN <sub>5</sub> ) (MeOH) <sub>2</sub> ]·MeOH	C <sub>14</sub> H <sub>22</sub> ClFeN <sub>5</sub> O <sub>3</sub> [Fe(HpydioneN <sub>5</sub> ) (MeOH)]	C <sub>38</sub> H <sub>52</sub> Fe <sub>2</sub> N <sub>16</sub> O <sub>5</sub> [Fe(pydioneN <sub>5</sub> ) (1-MeIm) <sub>2</sub> O ·2CH <sub>3</sub> CN	C <sub>34</sub> H <sub>56</sub> Cl <sub>2</sub> Fe <sub>2</sub> N <sub>10</sub> O <sub>9</sub> S <sub>4</sub> [Fe(pyCldioneN <sub>5</sub> ) (DMSO)] <sub>2</sub> O ·2DMSO
formula weight	427.29	397.65	461.73	399.67	924.66	1059.73
space group	<i>P2<sub>1</sub>/n</i>	<i>Pna2<sub>1</sub></i>	<i>P2<sub>1</sub>/c</i>	<i>P2<sub>1</sub>/n</i>	<i>P2<sub>1</sub>/n</i>	<i>P2<sub>1</sub>/n</i>
<i>a</i> , Å	10.396(3)	8.3892(5)	10.492(3)	8.6336(9)	11.730(2)	9.895(3)
<i>b</i> , Å	15.702(4)	18.6742(10)	16.550(4)	13.7092(15)	13.834(3)	14.405(4)
<i>c</i> , Å	12.084(3)	10.7301(6)	24.814(6)	14.7841(15)	25.885(5)	16.275(4)
$\alpha$ , deg	90	90	90	90	90	90
$\beta$ , deg	106.979(5)	90	94.536(6)	110.904(2)	95.722(5)	104.088(5)
$\gamma$ , deg	90	90	90	90	90	90
<i>V</i> , Å <sup>3</sup>	1886.6(9)	1680.99(16)	4295.5(18)	1718.2(3)	4179.5(14)	2249.9(10)
<i>Z</i>	4	4	8	4	4	2
<i>T</i> , K	213(2)	173(2)	213(2)	213(2)	173(2)	173(2)
$\lambda$ , Å	0.71073	0.71073	0.71073	0.71073	0.71073	0.71073
<i>D</i> <sub>calcd</sub> , g·cm <sup>-3</sup>	1.504	1.571	1.428	1.545	1.469	1.564
$\mu$ , mm <sup>-1</sup>	0.838	1.080	0.862	1.056	0.759	1.011
final <i>R</i> indices	<i>R</i> = 0.0461	<i>R</i> = 0.0257	<i>R</i> = 0.0991	<i>R</i> = 0.0290	<i>R</i> = 0.0893	<i>R</i> = 0.0657
[ <i>I</i> > 2 $\sigma$ ( <i>I</i> )] <sup>a</sup>	<i>wR</i> <sub>2</sub> = 0.0923	<i>wR</i> <sub>2</sub> = 0.0704	<i>wR</i> <sub>2</sub> = 0.2288	<i>wR</i> <sub>2</sub> = 0.0792	<i>wR</i> <sub>2</sub> = 0.2241	<i>wR</i> <sub>2</sub> = 0.1595
final <i>R</i> indices	<i>R</i> = 0.0950	<i>R</i> = 0.0266	<i>R</i> = 0.1527	<i>R</i> = 0.0329	<i>R</i> = 0.1855	<i>R</i> = 0.1432
[for all data] <sup>a</sup>	<i>wR</i> <sub>2</sub> = 0.1015	<i>wR</i> <sub>2</sub> = 0.0716	<i>wR</i> <sub>2</sub> = 0.2498	<i>wR</i> <sub>2</sub> = 0.0812	<i>wR</i> <sub>2</sub> = 0.2809	<i>wR</i> <sub>2</sub> = 0.1903

$$^a R = \sum |F_o| - |F_c| / \sum |F_o|. wR_2 = \{ \sum [w(F_o^2 - F_c^2)^2] / \sum [w(F_o^2)] \}^{1/2}.$$

toward a larger number of water molecules per molecule of the  $\mu$ -oxo dimer than the X-ray diffraction studies showed, which can be attributed to the different handling of the samples.

**X-ray Crystallographic Data.** A suitable crystal was chosen and was mounted on a glass fiber using Paratone-N oil. Data were measured using  $\omega$  scans of 0.3° per frame for 30 s, such that a hemisphere was collected. The first 50 frames were re-collected at the end of data collection to monitor for decay. Some of the complexes contained additional molecules of non-coordinated solvents in the lattice; these solvent molecules are specifically listed in Table 1, but they are omitted in the text of the paper. For Fe(pydioneN<sub>5</sub>)(MeOH)<sub>2</sub>, Fe(HpydioneN<sub>5</sub>)(Cl), and Fe(pyCldioneN<sub>5</sub>)(MeOH)<sub>2</sub>, the data were collected using a Bruker APEX CCD based diffractometer that was equipped with an LT-3 low-temperature apparatus operating at 213 K. A total of 1271 frames were collected with a maximum resolution of 0.75 Å. For Fe(pyCldioneN<sub>5</sub>)(MeOH), [Fe(pydioneN<sub>5</sub>)(1-MeIm)]<sub>2</sub>O, and [Fe(pyCldioneN<sub>5</sub>)(DMSO)]<sub>2</sub>O, the data were collected using a Bruker SMART CCD based diffractometer that was equipped with an LT-2 low-temperature apparatus operating at 173 K. A total of 1650 frames were collected with a maximum resolution of 0.75 Å.

Cell parameters were retrieved using SMART software<sup>40</sup> and were refined using SAINT<sup>41</sup> on all observed reflections. Data reduction was performed using the SAINT software,<sup>41</sup> which corrects for Lorentz, polarization, and decay effects. The structures were solved by the direct method using the SHELXS-97 program,<sup>42</sup> and they were refined by a least-squares method on *F*<sup>2</sup> by SHELXL-97,<sup>43</sup> which was incorporated in SHELXTL-PC V 5.10.<sup>44</sup> All drawings are done at 50% ellipsoids.

The structures of Fe(pydioneN<sub>5</sub>)(MeOH)<sub>2</sub>, Fe(pyCldioneN<sub>5</sub>)(MeOH)<sub>2</sub>, [Fe(pydioneN<sub>5</sub>)(1-MeIm)]<sub>2</sub>O, and [Fe(pyCldioneN<sub>5</sub>)(DMSO)]<sub>2</sub>O were solved in the space group *P2<sub>1</sub>/c* (# 14) by analysis

of systematic absences. All non-hydrogen atoms were refined anisotropically. Hydrogens (except for those bound to oxygen and nitrogen atoms, which were found on a difference Fourier map and were refined isotropically) were calculated by geometrical methods and were refined as a riding model.

The structure of Fe(pyCldioneN<sub>5</sub>)(MeOH) was solved in the space group *Pna2<sub>1</sub>* (No. 33) by analysis of systematic absences. Infinite chains of metal-containing fragments are observed in the crystal structure. Hydrogen atoms were located on a Fourier difference map and were refined isotropically, except for the methanol methyl group hydrogen atoms that were calculated by geometrical methods and were refined as a riding model.

The non-coordinated DMSO molecule in the structure of [Fe(pyCldioneN<sub>5</sub>)(DMSO)]<sub>2</sub>O was found to be disordered and was refined over two positions, where carbon atoms were restrained to have the same positions and anisotropic displacement parameters. The occupancies of the two sites converged at 0.556(19) and 0.444(19). All drawings are done at 50% ellipsoids.

The crystals used for the diffraction study showed no decomposition during data collection. Crystal data collection and refinement parameters are given in Table 1.

**Electrochemical experiments.** The cyclic voltammetry (CV) experiments were done in a glove box, under an argon atmosphere, in dry dimethylsulfoxide (0.1 M tetra-*N*-butylammonium perchlorate was used as a supporting electrolyte), with a CHI830 electrochemical analyzer (CHI Instruments, Inc.), and using a three-electrode cell with a pyrolytic graphite disk working electrode and platinum wires as both the counter electrode and the reference electrode. Potentials were determined using ferrocene as an internal standard and are reported relative to a saturated calomel electrode (SCE). The following procedure was employed to recalculate the observed potentials versus Cp<sub>2</sub>Fe<sup>+0</sup> to potentials versus SCE. Under the same experimental conditions, potentials of the Cp<sub>2</sub>Fe<sup>+0</sup> couple were measured in DMSO using a three-electrode cell with a pyrolytic graphite disk working electrode, a platinum wire as counter electrode, and an SCE as the reference electrode. The potential of the Cp<sub>2</sub>Fe<sup>+0</sup> couple was found to be +0.44 V versus SCE in DMSO, which is consistent with the literature data.<sup>45</sup> A conversion coefficient based on this value was applied to potentials versus the Cp<sub>2</sub>Fe<sup>+0</sup> couple.

(45) Vasudevan, D.; Wendt, H. J. *Electroanal. Chem.* **1995**, *192*, 69–74.

(40) SMART V 5.050 (NT) Software for the CCD Detector System; Bruker Analytical X-ray Systems: Madison, WI 1998.

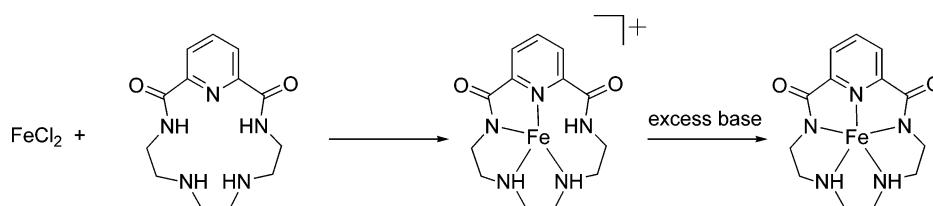
(41) SAINT V 5.01 (NT) Software for the CCD Detector System; Bruker Analytical X-ray Systems: Madison, WI 1998.

(42) Sheldrick, G. M. SHELXS-90, Program for the Solution of Crystal Structure, University of Göttingen, Germany, 1990.

(43) Sheldrick, G. M., SHELXL-97, Program for the Refinement of Crystal Structure; University of Göttingen, Germany, 1997.

(44) SHELXTL 5.10 (PC-Version) Program library for Structure Solution and Molecular Graphics; Bruker Analytical X-ray Systems: Madison, WI, 1998.

Scheme 2



**Mössbauer and Magnetic Susceptibility Studies.** Direct current (DC) and alternating current (AC) magnetic susceptibility measurements were made on polycrystalline powder samples using a Quantum Design (MPMSXL) superconducting quantum interference device (SQUID) magnetometer at Northeastern University. Magnetic susceptibilities were corrected for the background signal of the sample holder and for the diamagnetic susceptibilities of all atoms. AC susceptometry measurements were made using a Lake Shore Cryotronics Co. model 7000 AC susceptometer at Northeastern University. AC measurements on powdered samples were made over the temperature range of 4.2–30 K in an AC field of 1 Oe amplitude at a frequency of 125 Hz, and for higher temperatures, measurements were taken at 2.5 Oe at 500 Hz.

The Mössbauer spectra were determined using a conventional constant acceleration spectrometer operated in the multichannel scaling mode. The  $\gamma$ -ray source consisted of 51 mCi of  $^{57}\text{Co}$  in a rhodium metal matrix that was maintained at ambient temperature. The spectrometer was calibrated using a 6 micron thick natural abundance iron foil. Isomer shifts are reported relative to the center of the magnetic hyperfine pattern of the latter foil taken as zero velocity. The line widths of the innermost pair of  $\Delta M_1 = \pm 1$  transitions of the latter Zeeman pattern were reproducibly determined to be 0.214 mm/s. Sample temperature variation was achieved using a standard exchange gas liquid helium cryostat (Cryo Industries of America, Inc.), with temperature measurement and control based on silicon diode thermometry in conjunction with 10  $\mu\text{A}$  excitation sources (Lakeshore Cryotronics, Inc). Spectra were fit to unconstrained Lorentzians using the program ORIGIN PRO V 7.0 (Originlab, Inc.)

**Kinetic Measurements.** The kinetic measurements were performed using a Hi-Tech Scientific (presently, TgK Scientific, Salisbury, Wiltshire, U.K.) SF-43 cryogenic double-mixing stopped-flow instrument that is equipped with stainless steel plumbing, a 1.00 cm stainless steel mixing cell with sapphire windows, and an anaerobic gas-flushing kit. The instrument was connected to an IBM computer with IS-2 Rapid Kinetics Software by Hi-Tech Scientific. The mixing cell was maintained to  $\pm 0.1$  K, and the mixing time was 2–3 ms. The source of light was either a visible lamp combined with a monochromator (low-intensity light irradiation of the sample) or a xenon lamp combined with a diode array rapid scanning unit (strong UV–vis irradiation of the sample). To avoid contaminations with air, all manipulations with the iron complexes and their solutions were done using an argon atmosphere glovebox, gastight syringes, and the anaerobic stopped-flow instrument. Saturated solutions of  $\text{O}_2$  in  $\text{CH}_3\text{OH}$ ,  $\text{CH}_3\text{CN}$ , and mixtures of DMSO/dimethylformamide (DMF) with  $\text{CH}_3\text{CN}$  were prepared by bubbling with dry  $\text{O}_2$  gas for 10 min in a septum-closed cylinder with the solvent at a constant temperature (25  $^\circ\text{C}$ ). The solubility of  $\text{O}_2$  at 25  $^\circ\text{C}$  was accepted to be 8.4 mM in methanol and 8.1 mM in acetonitrile.<sup>46–48</sup> The solubility of dioxygen in mixtures of acetonitrile with DMF and DMSO (up to 10% v/v) was assumed to be equal to the solubility of dioxygen in pure acetonitrile. Solutions with lower  $\text{O}_2$  concentrations were prepared in gastight syringes by dilution of the saturated solution of oxygen with a corresponding

amount of the solvent containing no dissolved oxygen. The solutions of an iron(II) complex and  $\text{O}_2$  were cooled to a preset temperature in the stopped-flow instrument before mixing. The concentrations of the reactants were corrected for the 1:1 mixing ratio.

Kinetic data are summarized in the main text and in Tables S1–S13 and Figures S2–S10 (Supporting Information). A description of the fitting procedures is also given in Supporting Information.

## Results and Discussion

Macrocyclic ligands **1** and **1a** readily react with iron(II) salts. One or both amide groups can be deprotonated in the resulting complex. The fairly large macrocyclic cavity allows for the isolation of both mono- and dideprotonated complexes of iron(II), depending on the amount of weak non-coordinating base added (Scheme 2).

Mixing the iron(II) salt with the ligand **1** results in partial deprotonation (presumably with the macrocycle itself serving as a base) of the ligand that can be monitored by growth of the metal-to-ligand charge transfer (MLCT) band at  $\sim 580$  nm (Figure S11, Supporting Information). The monodeprotonated complex  $\text{Fe}(\text{HpydioneN}_5)(\text{Cl})$  can be obtained by a simple reaction of iron(II) chloride with **1** in methanol without the addition of base. Because of its relatively low solubility, the monodeprotonated complex  $\text{Fe}(\text{HpydioneN}_5)(\text{Cl})$  precipitates out of the solution in an analytically pure form.

To obtain the fully deprotonated complex, a non-coordinating base such as triethylamine must be added to the solution. The MLCT band at 580 nm reaches  $\sim 95\%$  of its maximum intensity at ca. 2 equiv of base added and levels off at ca. 4 equiv of triethylamine (Figure S11, Supporting information).

For **1a** it was possible to obtain two polymorphic modifications of the Fe(II) complex with the dideprotonated form of the ligand. A polymorph with two coordinated methanol molecules ( $[\text{Fe}(\text{pyCldioneN}_5)(\text{MeOH})_2]$ ) was obtained from dilute solutions of the complex in methanol by ether diffusion, and a polymorphic modification characterized by axial coordination of the amide oxygen of the neighboring molecule ( $[\text{Fe}(\text{pyCldioneN}_5)(\text{MeOH})]$ ) was obtained by slow evaporation of the concentrated methanol solutions in the glove box. The chemical behavior of the two polymorphs in solution is identical.

(46) *Oxygen and Ozone*; Battino, R., Ed.; Solubility Data Series, Pergamon Press: New York, 1981; Vol. 7.

(47) Achord, J. M.; Hussey, C. L. *Anal. Chem.* **1980**, *52*, 601–602.

(48) Sawyer, D. T.; Chiericato, G.; Angelis, C. T.; Nanni, E. J.; Tsuchiya, T. *Anal. Chem.* **1982**, *54*, 1720–1724.

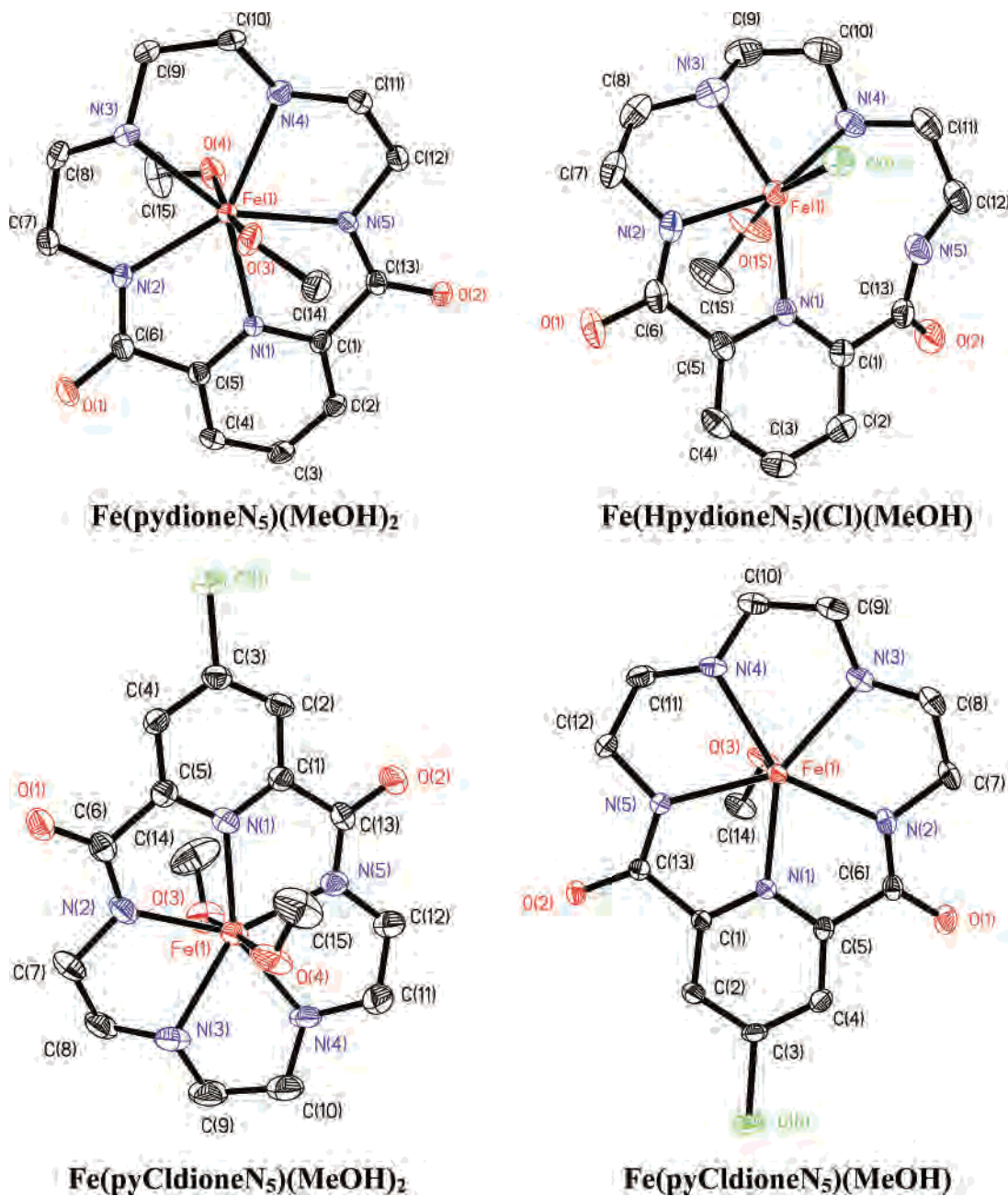


**Figure 1.** ORTEP plots of the synthesized iron(II) complexes (non-coordinated solvent molecules are omitted for clarity).

The protonation state of the synthesized complexes was additionally confirmed by analytical, spectroscopic, and structural data (vide infra).

**Structural features.** Both mono- and dideprotonated complexes of Fe(II), as well as the Fe(III)  $\mu$ -oxo dimers that are the final products of oxidation in aprotic solvents, were characterized by X-ray crystallography. Oak Ridge thermal ellipsoid plots (ORTEP) of the complexes are shown in Figures 1 and 2; these figures, as well as the discussion below, focus on the coordination sphere of the metal and do not include non-coordinated solvent molecules.

Dideprotonated complexes of both the iron(II) and the iron(III)  $\mu$ -oxo dimers exhibit a pentagonal–bipyramidal coordination mode, which is analogous to the previously described Fe(III) complex of **1**.<sup>25</sup> For all dideprotonated

compounds, the coordination polyhedron of iron(II) is a nearly perfect pentagonal-bipyramid with five nitrogen atoms of the ligand in the equatorial plane and with two molecules of methanol in the axial positions; the maximum deviations from the mean plane of all nitrogen atoms are less than 0.2 Å (Table 2). Such coordination geometry is rare (according to Casanova et al., heptacoordinate complexes constitute 1.8% of all  $\sigma$ -bonded transition complexes reported in the Cambridge Crystallographic Data Centre (CCDC)<sup>49</sup>), and it is normally enforced by the structure of the ligand.<sup>50,51</sup> Ligand

(49) Casanova, D.; Alemany, P.; Bofill, J. M.; Alvarez, S. *Chem.—Eur. J.* **2003**, *9*, 1281–1295.

(50) Ivanovic-Burmazovic, I.; Andjelkovic, K. *Adv. Inorg. Chem.* **2004**, *55*, 315–360.

(51) Steitz, M.; Kaiser, A.; Stempfhuber, S.; Zabel, M.; Reiser, O. *Inorg. Chem.* **2005**, *44*, 4630–4636.

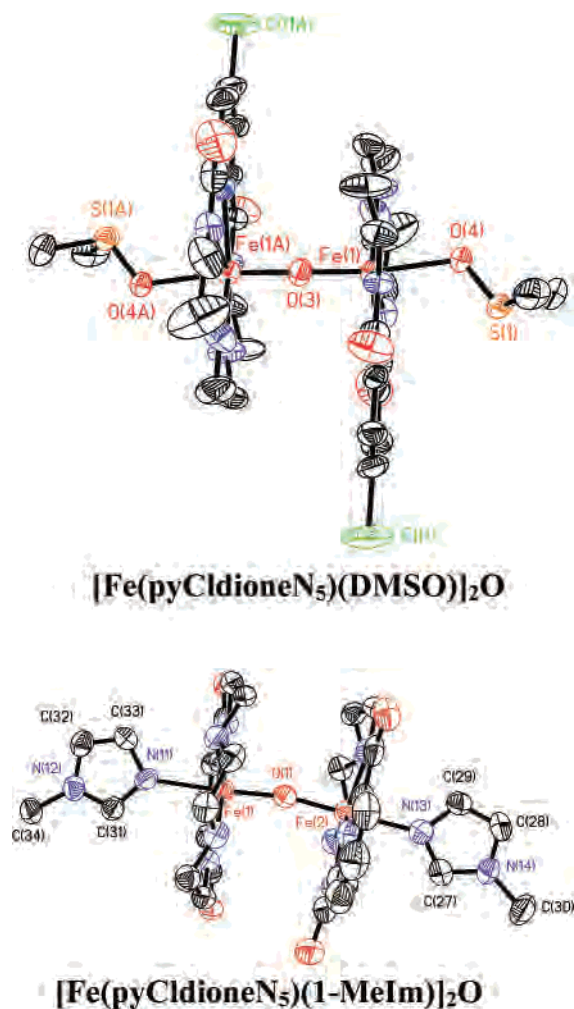


**Figure 2.** ORTEP plots of the iron(III)  $\mu$ -oxo dimers, the final products of oxygenation (non-coordinated solvent molecules are omitted for clarity).

**1**<sup>25</sup> and related macrocycles<sup>52,53</sup> are known to create an environment that is well suited for such a coordination mode.

The average (for two molecules in the asymmetric unit) distance of Fe–N<sub>py</sub> in Fe(pyCldioneN<sub>5</sub>)(MeOH)<sub>2</sub> is 2.177(3) Å, as compared to 2.203(2) Å in Fe(pydioneN<sub>5</sub>)(MeOH). Introducing an electron-withdrawing chlorine atom in the  $\gamma$  position of the pyridine ring results in slight shortening of the bond, which might be explained by facilitated  $\pi$ -back-donation to the ring. The opposite trend is observed for the Fe–N<sub>amide</sub> distance; in Fe(pydioneN<sub>5</sub>)(MeOH)<sub>2</sub>, the average Fe–N<sub>amide</sub> distance (2.189(6) Å) is shorter than that in Fe(pyCldioneN<sub>5</sub>) (2.211(4) Å). The Fe–N<sub>amine</sub> distances in Fe(pydioneN<sub>5</sub>)(MeOH)<sub>2</sub> (2.32(1) Å) and in Fe(pyCldioneN<sub>5</sub>) (2.317(9) Å) are essentially the same. It should be noted that two polymorphic modifications of Fe(pyCldioneN<sub>5</sub>) were obtained. Both polymorphs have very similar geometric parameters and differ only by the number of methanol molecules coordinated to the iron atom. In Fe(pyCldioneN<sub>5</sub>)(MeOH)<sub>2</sub>, two methanol molecules serve as axial ligands, whereas, in Fe(pyCldioneN<sub>5</sub>)(MeOH), an amide oxygen atom

from the neighboring molecule acts as one of the axial ligands to form infinite chains of metal-containing fragments (Figure 3).

The solid-state structure of the monodeprotonated complex Fe(HpydioneN<sub>5</sub>)(Cl) is fairly different. The iron atom has a pseudo-octahedral environment that is comprised of the pyridine nitrogen, a deprotonated amide nitrogen, two amine nitrogens in the equatorial plane, and a chloride anion and an oxygen atom from a coordinated methanol molecule in the axial positions. Interestingly, the Fe–N<sub>py</sub> distance in Fe(HpydioneN<sub>5</sub>)(Cl) is also 2.1999(11) Å, so the change of coordination number, in this case, does not result in a shortening of the Fe–N<sub>py</sub> bond. However, the Fe–N<sub>amide</sub> bond is much shorter in the monodeprotonated complex (2.0837(11) Å), and the average Fe–N<sub>amine</sub> distance in Fe(HpydioneN<sub>5</sub>)(Cl) is also significantly shorter (2.2250(13) Å), which corresponds to a geometrically less constrained state.

The Fe–N<sub>amide</sub> bond length in Fe(HpydioneN<sub>5</sub>)(Cl) agrees well with the values observed for a high-spin pseudo-octahedral Fe(II) complex with *N*-(bis(2-pyridyl)methyl)pyridine-2-carboxamide (2.0690(14) and 2.090(2) Å),<sup>35</sup> and it is significantly longer than the Fe–N<sub>amide</sub> bond in a sterically unhindered low-spin Fe(II) complex with PrpepH (PrpepH = *N*-(2-(4-imidazolyl)ethyl)pyrimidine-4-carboxamide) (1.989(6) Å).<sup>23</sup>

It should be noted that iron–nitrogen distances do not differ significantly in iron(II) and iron(III) complexes with dideprotonated ligands. The average distance Fe(II)–N<sub>py</sub> is essentially the same (2.203(2) Å) as in the case of the Fe(III) complex Fe(pydioneN<sub>5</sub>)(Cl) (2.193(4) Å).<sup>25</sup> This distance is an essentially constant value, and it is independent of the nature of the axial ligand in the case of Fe(III), as can be seen from Table 2. The average Fe–N<sub>amide</sub> and Fe–N<sub>amine</sub> distances are longer (by approximately 0.03 and 0.05 Å, respectively) in the iron(II) complex than the corresponding distances in the iron(III) complex.

**Mössbauer and Magnetic Susceptibility Data.** The ambient temperature Mössbauer spectra of the pure iron(II) complexes with **1** consist of a single quadrupole doublet that indicates the presence of only one type of iron, which is in accord with the solid-state structures (Figure 4 and Figures S12–S16 in Supporting Information). The isomer shift and quadrupole splitting for the monodeprotonated complex Fe(HpydioneN<sub>5</sub>)(Cl) are  $\delta = 1.16$  mm/s and  $\Delta E_Q = 2.59$  mm/s ( $\delta = 1.28$  mm/s and  $\Delta E_Q = 3.11$  mm/s at 77.5 K). The parameters for the dideprotonated complex Fe(pydioneN<sub>5</sub>) are  $\delta = 1.24$  mm/s and  $\Delta E_Q = 2.32$  mm/s at 293 K. These results are fully consistent with the expected systematic (for <sup>57</sup>Fe) increasing of the isomer shift with an increasing of coordination number.<sup>54</sup> The isomer shift and the quadrupole splitting for the Fe(pyCldioneN<sub>5</sub>)(MeOH) are  $\delta = 1.42$  mm/s  $\Delta E_Q = 2.83$  mm/s ( $\delta = 1.54$  mm/s and  $\Delta E_Q = 2.90$  mm/s at 77.5 K). The value of the quadrupole splitting for the seven coordinate complex Fe(pydioneN<sub>5</sub>) is similar to those of the

(52) Drew, M. G. B.; bin Othman, A. H.; McIlroy, P. D. A.; Nelson, S. M. *J. Chem. Soc. Dalton Trans.* **1975**, 2507–2516.

(53) Drew, M. G. B.; Rice, D. A.; Bin Silong, S. *Polyhedron* **1983**, *2*, 1053–1056.

(54) Greenwood, N. N.; Gibb, T. C. *Mössbauer Spectroscopy*; Chapman and Hill: London, 1971.

**Table 2.** Selected Bond Lengths (Å) and Angles (deg) for Crystallographically Characterized Complexes

bond, Å/angle, deg	[Fe(pydioneN <sub>5</sub> )(MeOH) <sub>2</sub> ]	[Fe(pyCldioneN <sub>5</sub> )(MeOH)]	[Fe(pyCldioneN <sub>5</sub> )(MeOH) <sub>2</sub> ]	[Fe(HpydioneN <sub>5</sub> )(Cl)(MeOH)]	[Fe(pyCldioneN <sub>5</sub> )(1-Melm) <sub>2</sub> O]	[Fe(pyCldioneN <sub>5</sub> )(DMSO) <sub>2</sub> O]
Fe–N <sub>py</sub>	2.203(2)/N1	2.1714(14)/N1	2.179(6)/N1 2.181(5)/N6	2.1999(11)/N1	2.197(4)/N1 2.197(5)/N6	2.193(4)/N1
Fe–N <sub>amide</sub>	2.183(3)/N2 2.195(3)/N5	2.2091(15)/N2 2.2204(13)/N5	2.208(6)/N2 2.199(6)/N5 2.207(5)/N7 2.223(6)/N10	2.0837(11)/N2	2.195(5)/N2 2.184(5)/N5 2.169(5)/N7 2.198(5)/N10	2.179(4)/N2 2.164(4)/N5
Fe–N <sub>amine</sub>	2.311(3)/N4 2.338(3)/N3	2.2813(16)/N4 2.3332(13)/N3	2.304(6)/N4 2.333(6)/N3 2.314(6)/N8 2.339(6)/N9	2.2073(13)/N3 2.2426(12)/N4	2.2705(13)/N3 2.280(5)/N3 2.321(5)/N8 2.297(5)/N9	2.268(4)/N4 2.262(4)/N3
Fe–L <sub>ax</sub>	2.235(2)/O3 2.320(3)/O4	2.1800(13)/O3 2.2948(12)/O2#	2.201(6)/O3 2.207(6)/O4 2.222(5)/O7 2.234(5)/O8	2.4892(4)/Cl1 2.2792(11)/O1S	1.815(3)/O1–Fe1 1.817(3)/O1–Fe2 2.271(5)/N11–Fe1 2.246(5)/N13–Fe2	1.7907(8)/O3 2.237(3)/O4
C=O	1.272(3)/O2 1.267(4)/O1	1.2751(17)/O2 1.261(2)/O1	1.266(8)/O1 1.281(8)/O2 1.282(8)/O5 1.284(8)/O6	1.2705(15)/O1 1.2260(17)/O2	1.247(5)/O2 1.268(7)/O3 1.259(7)/O4 1.246(8)/O5	1.263(6)/O2 1.251(5)/O1
C <sub>amide</sub> –N <sub>amide</sub>	1.310(4)/N2 1.308(4)/N5	1.301(3)/N2 1.335(2)/N5	1.306(9)/N2 1.306(8)/N5 1.294(8)/N7 1.298(9)/N10	1.2984(18)/N2 1.3385(19)/N5	1.247(9)/N2 1.304(8)/N2 1.323(8)/N5 1.330(8)/N7 1.316(8)/N10	1.307(6)/N2 1.302(7)/N5
C <sub>amide</sub> –C <sub>py</sub>	1.508(4)/C6 1.504(4)/C13	1.508(2)/C6 1.494(2)/C13	1.519(9)/C6 1.505(9)/C13 1.504(9)/C21 1.493(9)/C28	1.5004(18)/C6 1.5052(17)/C13	1.505(9)/C6 1.492(9)/C13 1.462(9)/C19 1.485(9)/C26	1.508(4)/C6 1.504(4)/C13
N <sub>py</sub> –Fe–N <sub>amide</sub>	71.60(9)/ N1–Fe–N2 70.70(9)/ N1–Fe–N5	71.38(5)/ N1–Fe–N2 70.69(5)/ N1–Fe–N5	71.5(2)/ N1–Fe1–N2 71.0(2)/ N1–Fe1–N5 71.4(2)/ N6–Fe1–N7 71.2(2)/ N6–Fe1–N10	75.32(4)	71.33(18)/ N1–Fe1–N2 71.01(18)/ N1–Fe1–N5 71.9(2)/ N6–Fe2–N7 70.4(2)/ N6–Fe2–N10	70.51(13)/ N1–Fe–N2 71.32(15)/ N1–Fe–N5
N <sub>amide</sub> –Fe–N <sub>amine</sub>	72.34(9)/ N2–Fe–N3 72.65(9)/ N4–Fe–N5	72.02(6)/ N2–Fe–N3 72.98(5)/ N4–Fe–N5	71.0(1)/ N2–Fe–N3 73.5(2)/ N4–Fe–N5 72.64(19)/ N7–Fe–N8 71.8(2)/ N9–Fe–N10	76.91(5)	72.64(17)/ N2–Fe–N3 71.33(18)/ N4–Fe–N5 72.98(18)/ N7–Fe–N8 71.2(2)/ N9–Fe–N10	72.28(15)/ N2–Fe–N3 72.77(18)/ N4–Fe–N5
N <sub>amine</sub> –Fe–N <sub>amine</sub>	73.61(9)	73.41(5)	73.6(2)/ N3–Fe–N4 73.6(2)/ N8–Fe–N9	79.35(5)	73.32(18)/ N3–Fe–N4 73.22(19)/ N8–Fe–N9	72.00(17)
L <sub>ax</sub> –Fe–L <sub>ax</sub>	171.78(9)	161.72(6)	175.0(2)/ O3–Fe1–O4 171.5(2)/ O7–Fe2–O8	167.10(4)	176.55(17)/ O1–Fe1–N11 175.59(16)/ O1–Fe2–N13	172.61(9)
Fe(1)–O–Fe(2) maximum out-of-plane (defined by the five nitrogen atoms) deviation of N atoms/displacement of Fe atom	0.170(2) N4/ 0.0111(16)	0.1277(9) N2/ 0.0415(7)	0.136(4) N3/ 0.020(3) Fe1 0.133(4) N9/ 0.011(3) Fe2	0.2821(7) N5/ 0.0251(6)	0.135(3) N3/ 0.159(3) Fe1 0.106(3) N9/ 0.128(2) Fe2	0.083(3) N5/ 0.179(2)

Schiff base seven coordinate macrocyclic complexes reported by Drew et al.,<sup>55</sup> however, the isomer shift is ca. 0.1–0.2 mm/s higher for iron(II) complexes of H<sub>2</sub>pydioneN<sub>5</sub>.

All iron(II) complexes remain in a high-spin state upon cooling to 77.5 K. This has also been supported by the AC magnetic susceptibility data; plots of the temperature dependence of the magnetic susceptibility for iron(II) complexes are given in Supporting Information (Figures S17–S21). The effective magnetic moment of Fe(pydioneN<sub>5</sub>) at room-temperature is 5.1  $\mu_{\beta}$ , which is consistent with the

values reported for the closely related seven coordinate iron(II) complexes.<sup>55,56</sup> The somewhat lower magnetic moment value (4.6  $\mu_{\beta}$ ) observed for Fe(pyCldioneN<sub>5</sub>)(MeOH) may suggest a weak antiferromagnetic exchange. The sudden drop of the magnetic moment at low-temperature suggests that zero-field splitting effects dominate in that range, which is common to high-spin iron(II).

(55) Drew, M. G. B.; Grimshaw, J.; McLroy, P. D. A.; Nelson, S. M. *J. Chem. Soc. Dalton. Trans.* **1976**, 1388–1394.

(56) Nelson, S. M.; McLroy, P. D. A.; Stevenson, C. S.; König, E.; Ritter, G.; Waigel, J. *J. Chem. Soc. Dalton. Trans.* **1986**, 991–995.



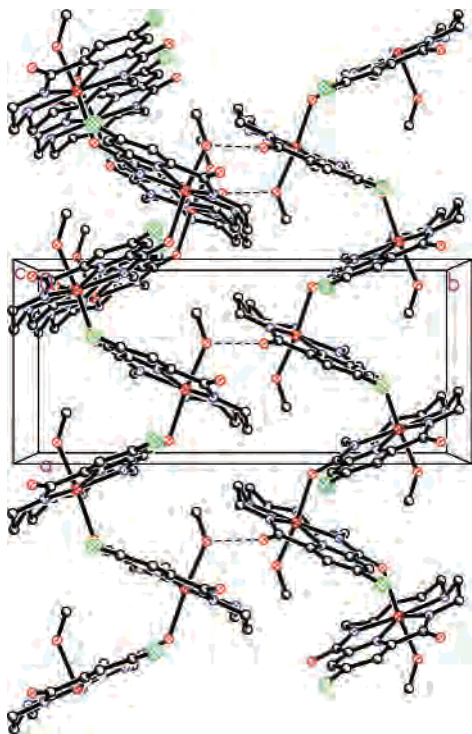


**Figure 3.** Packing diagram for Fe(pyCldioneN<sub>5</sub>)(MeOH) showing infinite chains of iron-containing fragments.

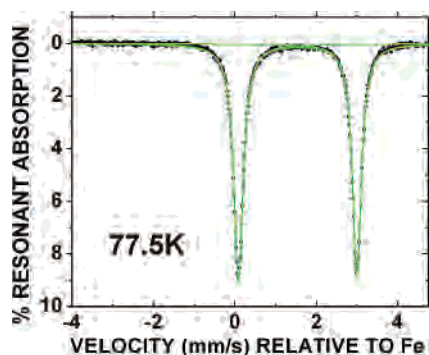


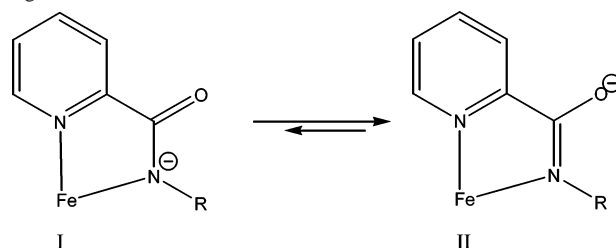
**Figure 4.** Mössbauer spectrum of Fe(pyCldioneN<sub>5</sub>)(MeOH) at 77.5 K.

Unlike the previously reported iron(III) complex, Fe(pydioneN<sub>5</sub>)(Cl),<sup>25</sup> cooperative effects due to the extensive network of hydrogen bonds in Fe(pydioneN<sub>5</sub>)(MeOH)<sub>2</sub> (Figure S22, Supporting Information) or due to bridging amide oxygen atoms for Fe(pyCldioneN<sub>5</sub>)(MeOH) (Figure 3) were not observed for the iron(II) complexes. In the case of Fe(pyCldioneN<sub>5</sub>)(MeOH), the Mössbauer spectrum at 7 K, in conjunction with the magnetization data, incontrovertibly shows that this material does not exhibit a long-range magnetic order, but rather it is a rapidly relaxing paramagnet to a temperature of  $\sim 1.8$  K.

**Spectroscopic Characterization.** The coordination of an amide-containing ligand to a metal can be additionally characterized by the shifts in the IR frequencies of the amide group.

The spectrum of the monodeprotonated complex Fe(HpydioneN<sub>5</sub>)(Cl) contains both the bands originating from both the non-coordinated amide group,  $1678\text{ cm}^{-1}$  ( $\nu\text{ C=O}$ ) and  $1537\text{ cm}^{-1}$  ( $\nu\text{ C-N}$ ), and the coordinated amide group,  $1614\text{ cm}^{-1}$  ( $\nu\text{ C=O}$ ) and  $1562\text{ cm}^{-1}$  ( $\nu\text{ C-N}$ ). In the didepro-

**Scheme 3.** Resonance Structures of the Coordinated Amidopyridine Fragment



nated complex, only the bands attributed to the deprotonated amide group can be observed,  $1612\text{ cm}^{-1}$  ( $\nu\text{ C=O}$ ) and  $1570\text{ cm}^{-1}$  ( $\nu\text{ C-N}$ ). Comparison of the data with previously reported values<sup>25</sup> for the iron(III) complex of **1** ( $1621\text{ cm}^{-1}$  ( $\nu\text{ C=O}$ ) and  $1561\text{ cm}^{-1}$  ( $\nu\text{ C-N}$ )) shows a slightly higher contribution of the resonance form II for the iron(II) complex, which is in agreement with the study by Mascharak and co-workers (Scheme 3).<sup>23</sup>

The UV–visible spectrum of Fe(pydioneN<sub>5</sub>) in DMSO is presented in Figure S23, Supporting Information. The purple color of the complex is attributed to a MLCT band with a maximum at 602 nm ( $\epsilon = 1200\text{ M}^{-1}\cdot\text{cm}^{-1}$ ) in DMSO. Interestingly, the band exhibits both thermo- and solvatochromic behavior; the maximum of the band undergoes a red shift of ca. 30 nm upon cooling the solution of Fe(pydioneN<sub>5</sub>) in methanol down to  $-80\text{ }^\circ\text{C}$ . The thermo-chromic behavior cannot be attributed to changes in the spin state of iron upon cooling, as the complex remains in the high-spin state even at liquid helium temperature (vide supra). Solvatochromism of Fe(pydioneN<sub>5</sub>) is also pronounced; the MLCT band maximum ranges from 515 nm in a DMF/CH<sub>3</sub>CN 8:92 v/v mixture to 600 nm in pure DMSO. The position of the band generally correlates with the electron-donating ability of the solvent.

The position of the MLCT band in Fe(pyCldioneN<sub>5</sub>) (maximum at 645 nm in DMSO) is also in agreement with the assignment; introduction of an electron-withdrawing substituent into the ring facilitates the charge transfer. Fe(pyCldioneN<sub>5</sub>) also exhibits thermo- and solvatochromic behavior analogous to that of Fe(pydioneN<sub>5</sub>). In both Fe(II) complexes the position of the maximum exhibit red shifts upon cooling, which is unlike the analogous Fe(III) complex that exhibited blue shift of the LMCT band upon cooling.<sup>25</sup>

The UV–vis spectrum of Fe(HpydioneN<sub>5</sub>)(Cl) has similar features; however, the MLCT band has a maximum at 574 nm and has an extinction coefficient of approximately half ( $550\text{ M}^{-1}\cdot\text{cm}^{-1}$ ) that of its dideprotonated analogue Fe(pydioneN<sub>5</sub>). This difference was used in the study of the deprotonation of the amide groups during complexation (vide supra).

**NMR.** To study the protonation state of the complexes in solution, we have also acquired their NMR spectra. The <sup>1</sup>H spectra of Fe(pydioneN<sub>5</sub>) (Figure 5) and Fe(pyCldioneN<sub>5</sub>) (Figure S24, Supporting Information) are very similar in DMSO-*d*<sub>6</sub>. It can be concluded from these spectra (by the presence of only one peak at  $\sim 40$  ppm in the spectrum of Fe(pyCldioneN<sub>5</sub>)) that the pyridine protons have chemical shifts in this region. At the same time, the <sup>1</sup>H NMR spectrum

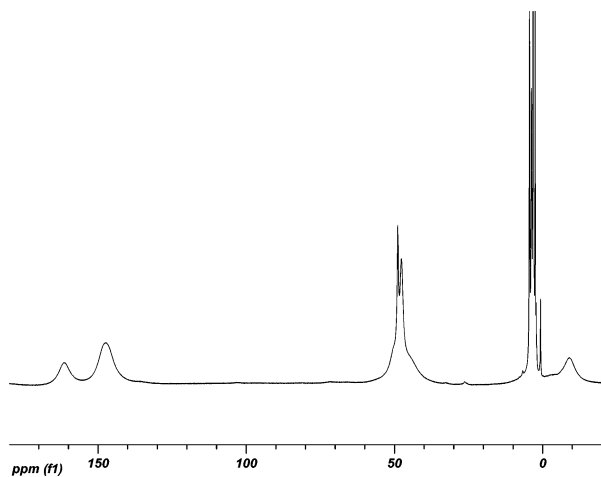


Figure 5.  $^1\text{H}$  NMR spectrum of  $\text{Fe}(\text{pydioneN}_5)$  in  $\text{DMSO}-d_6$ .

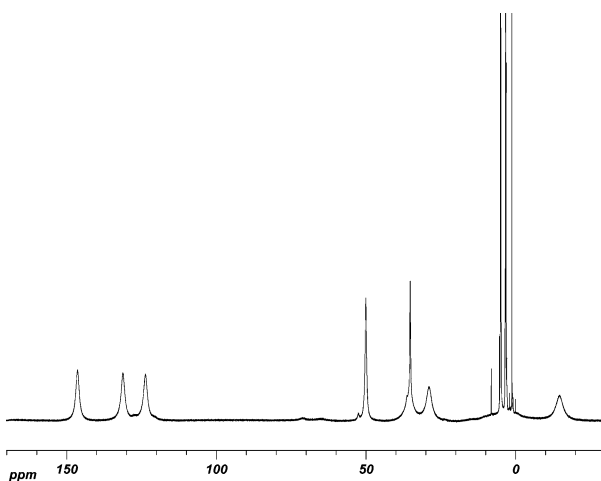


Figure 6.  $^1\text{H}$  NMR spectrum of  $\text{Fe}(\text{pydioneN}_5)$  in  $\text{CD}_3\text{OD}$ .

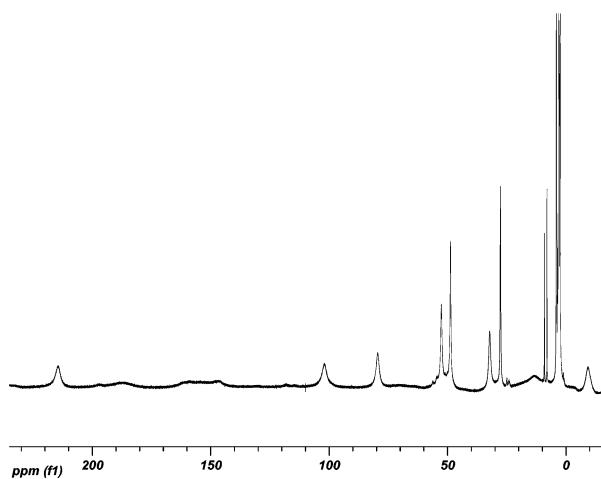


Figure 7.  $^1\text{H}$  NMR spectrum of  $\text{Fe}(\text{HpydioneN}_5)(\text{Cl})$  in  $\text{DMSO}-d_6$ .

of  $\text{Fe}(\text{HpydioneN}_5)(\text{Cl})$  in  $\text{DMSO}-d_6$  is completely different (Figure 7) and shows an effective doubling of signals, which we ascribe to the preservation of the six-coordinate coordination mode in solution. It also suggests a slow protonation–dissociation/deprotonation–coordination of the two amide groups; i.e., the  $\text{Fe}-\text{N}$  bond is not labile on the NMR time scale. The six-coordinated monodeprotonated species does not possess the symmetry elements present in the dide-

protonated seven-coordinate complex. The NMR spectra of  $\text{Fe}(\text{pydioneN}_5)$  and  $\text{Fe}(\text{pyCldioneN}_5)$  in  $\text{CD}_3\text{OD}$  are similar to those in  $\text{DMSO}-d_6$  (Figure 6 and Figure S25 in Supporting Information). The NMR study of the monodeprotonated complex  $\text{Fe}(\text{HpydioneN}_5)(\text{Cl})$  in methanol was hindered by its low solubility.

Such distinct differences between the NMR spectra of  $\text{Fe}(\text{HpydioneN}_5)(\text{Cl})$  and  $\text{Fe}(\text{pydioneN}_5)$  provide a useful spectroscopic tool for determining the protonation state of these complexes in solution.

**Electrochemistry.** The redox potential of  $\text{Fe}(\text{pydioneN}_5)$  is identical, within the experimental error, to the potential of the previously reported  $\text{Fe}(\text{III})$  complex,  $\text{Fe}(\text{pydioneN}_5)(\text{Cl})$ .<sup>25</sup> This can be viewed as the evidence, in the  $\text{Fe}(\text{III})$  case, that the  $\text{Cl}^-$  ligand is fully dissociated in the  $\text{DMSO}$  solution. We have also studied the electrochemical properties of the monodeprotonated complex by cyclic voltammetry and have found that its redox potential also equals  $-0.56$  mV versus SCE (Figures S26 and S27, Supporting Information). This can be explained by rapid deprotonation of the  $\text{Fe}(\text{III})$  complex during cyclic voltammetry scans, which is consistent with the fact that no monodeprotonated species was observed for the iron(III) complex.

The redox potential of the  $\text{Fe}^{3+}/\text{Fe}^{2+}$  couple in  $\text{Fe}(\text{pyCldioneN}_5)$  is  $-0.49$  V versus SCE in  $\text{DMSO}$ , which is consistent with the smaller electron donating ability of the chloro substituted ligand (Figure S28, Supporting Information).

**Stopped-Flow Kinetic Characterization of the Reactions of Iron(II) Complexes with Dioxygen.** In a methanol solution, the mono- and dideprotonated forms of the  $\text{Fe}(\text{II})$  complex of **1** ( $\text{Fe}(\text{HpydioneN}_5)(\text{Cl})$  and  $\text{Fe}(\text{pydioneN}_5)$ , respectively) appear to be in equilibrium, according to UV–vis data (the position of the maximum of the CT band and its extinction coefficient are a function of the concentration of the complex). At the same time, NMR studies (vide supra) suggest that  $\text{Fe}(\text{HpydioneN}_5)(\text{Cl})$  mostly preserves its monodeprotonated state in the  $\text{DMSO}$  solution. Both complexes are easily soluble in DMF,  $\text{DMSO}$ , pyridine, and 1-methylimidazole; however, they are not soluble, to an appreciable extent, in THF,  $\text{CH}_2\text{Cl}_2$ , or nitriles. Therefore, the kinetic characterization of the complexes in aprotic solvents was performed in solvent mixtures that contained  $<10\%$  of  $\text{DMSO}$  or DMF.

Oxygenation reactions of  $\text{Fe}(\text{pydioneN}_5)$  were studied using a cryogenic stopped-flow technique in various solvents and solvent mixtures. In methanol, the reaction of  $\text{Fe}(\text{pydioneN}_5)$  with  $\text{O}_2$  is very fast, and the reaction goes to completion within 5 s at  $-80$  °C and within 0.5 s at  $-60$  °C. Spectral changes and a kinetic trace for this reaction are presented in Figures 8 and 9, respectively. The initial spectrum after mixing looks very similar to that of the starting iron(II) complex.

The reaction is first-order both in  $\text{Fe}(\text{pydioneN}_5)$  and in dioxygen, as determined from the independence of the observed rate constant on the concentration of the complex and from a linear dependence of  $k_{\text{obs}}$  on the concentration of  $\text{O}_2$ , respectively. Activation parameters were determined

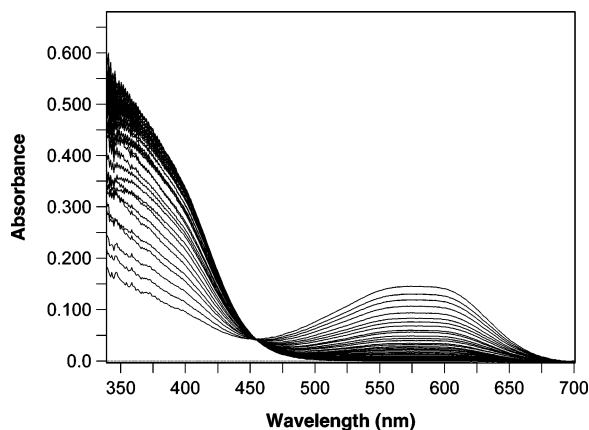


**Figure 8.** Time-resolved spectra acquired by the stopped-flow technique during the reaction of Fe(pydioneN<sub>5</sub>) (0.15 mM) with O<sub>2</sub> (4.2 mM) in methanol at  $-80$  °C over a 5 s time range.

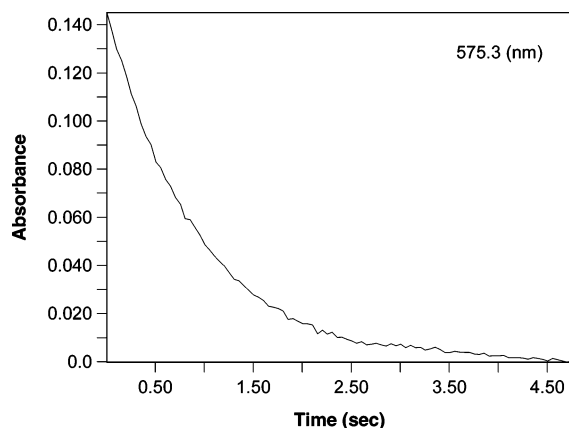
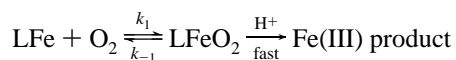


**Figure 9.** Kinetic trace of the reaction of Fe(pydioneN<sub>5</sub>) (0.15 mM) with O<sub>2</sub> (4.2 mM) in methanol at  $-80$  °C at 575.3 nm.

from the temperature dependence of the second-order rate constant,  $k$ , to be  $\Delta H^\ddagger = 24.9(5)$  kJ/mol and  $\Delta S^\ddagger = -56(2)$  J/mol·K (Figure S4, Supporting Information). These activation parameters are in agreement with an associative process; however, they should be interpreted with care because the reaction may be comprised of more than one elementary step.

These findings are consistent with the following mechanism:



The rate of formation of the iron(III) superoxo species, as extrapolated from the activation energy to  $-40$  °C ( $t_{1/2} \sim 8$  ms), is consistent with the rates estimated from oxygenation studies in aprotic solvent (vide infra). A similar behavior (rapid oxidation even at low temperatures) and the same kinetic rate law were both reported for the oxygenation of Fe(II) cyclidenes by Busch and co-workers.<sup>57</sup>

The oxygenation of Fe(pydioneN<sub>5</sub>) in aprotic solvents proceeds by a completely different mechanism. Unfortunately, the solubility of Fe(pydioneN<sub>5</sub>) in solvents such as acetonitrile, propionitrile, or THF is limited, so solvent mixtures were used; Fe(pydioneN<sub>5</sub>) was first dissolved in

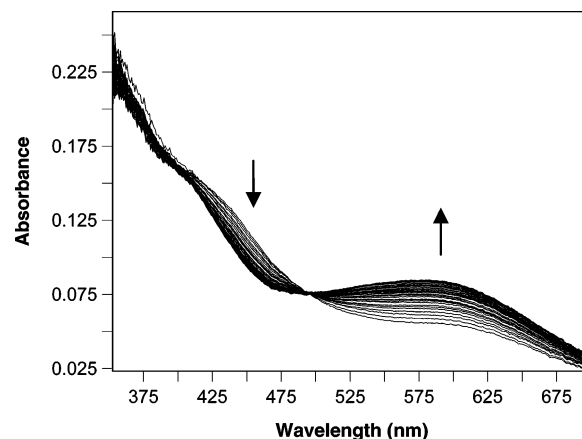
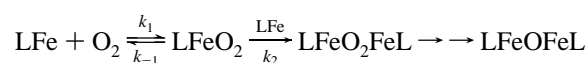


**Figure 10.** Time-resolved spectra acquired by the stopped-flow technique during the reaction of Fe(pydioneN<sub>5</sub>) (0.2 mM) with O<sub>2</sub> (4.1 mM) in DMF/CH<sub>3</sub>CN 8:92 v/v at  $-40$  °C over a 1 s time range.

DMSO, DMF, or 1-methyl-imidazole and then diluted with the second component. Normally, mixtures of either 8% v/v DMF or 10% v/v DMSO in acetonitrile were used for oxygenation studies in aprotic solvents. In all of the cases, the reaction proceeds via the same pathway; two kinetic processes were observed. The first process (intermediate formation) is very fast (complete in a few seconds at  $-40$  °C) and is followed by a slower (by approximately 2 orders of magnitude) intermediate decomposition process. The fast process is accompanied by an increase in absorption from ca. 450 to 700 nm (the exact position of the band depends on the solvent/solvent mixture, with the maximum in DMF/CH<sub>3</sub>CN 8:92 v/v at ca. 580 nm) and by a decrease in absorbance from 350 to 450 nm. The second, slower process is characterized by a decrease in absorbance from ca. 360–430 nm and by an increase in absorbance above ca. 430 nm (Figures 10 and 11). Exact positions of the isosbestic points are also dependent upon the solvent.

A detailed kinetic investigation of the oxygenation reaction was undertaken. According to the concentration dependence studies, the first step has a second-order dependence on Fe(pydioneN<sub>5</sub>). The kinetic traces, which were recorded in the presence of excess O<sub>2</sub>, were fit to a second-order rate law. These second-order rate constants were independent of the concentration of the iron(II) complex (while the initial reaction rates scaled as [FeL]<sup>2</sup>) (Table S4, Supporting Information). Interestingly, an increase in the dioxygen concentration resulted in a slower oxygenation reaction (Figure 12). The second step is first-order in Fe(pydioneN<sub>5</sub>) and is zero-order in O<sub>2</sub>. The final product of the reaction can be isolated and crystallographically characterized as a  $\mu$ -oxo dimer (Figure 2). Activation parameters that were determined for the reactions in different solvents are given in Table 3 (however, it should be mentioned that these are effective values, which do not correspond to individual reaction steps).

These findings are consistent with the reaction mechanism outlined below.



(57) Sauer-Masarwa, A.; Dickerson, L. D.; Herron, N.; Busch, D. H. *Coord. Chem. Rev.* **1993**, *128*, 117–137.

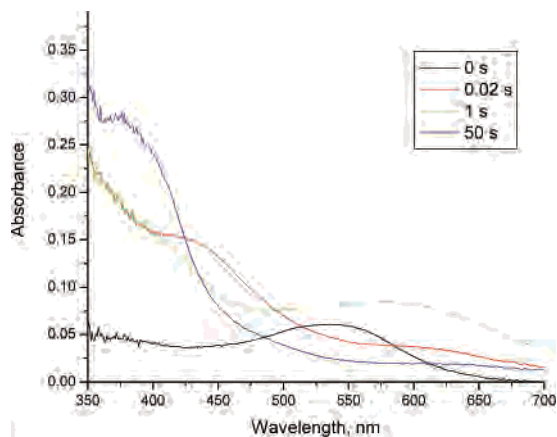


**Figure 11.** Overlay of UV-vis spectra of the reaction mixture at different times during the course of the reaction of Fe(pydioneN<sub>5</sub>) with O<sub>2</sub>. Obtained by the stopped-flow method at -40 °C in DMF/CH<sub>3</sub>CN 8:92 v/v. Black line, *t* = 0, starting Fe(pydioneN<sub>5</sub>); red line, *t* = 0.02 s, after mixing, the spectrum represents the iron superoxo species; green line, *t* = 1 s, formation of the diiron peroxo species is complete; blue line, *t* = 50 s, the decomposition of peroxospecies is almost complete, the reaction was monitored in the diode-array mode with substantial irradiation by UV light, which greatly facilitated the decomposition of the peroxide.

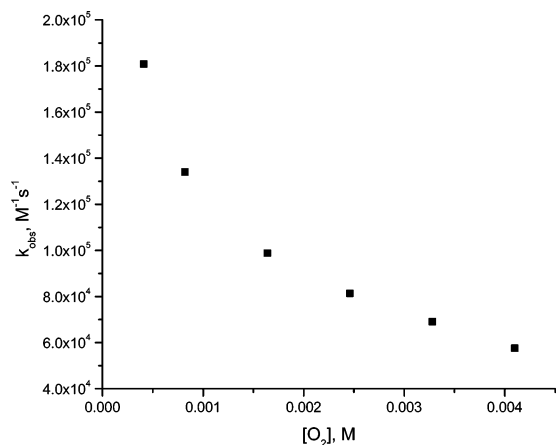


**Figure 12.** Plot of the observed rate constant of the reaction between complex Fe(pydioneN<sub>5</sub>) (0.25 mM) and O<sub>2</sub> in DMF/CH<sub>3</sub>CN 8:92 v/v in the presence of 50 equiv of 1-methylimidazole at -40 °C at different initial concentrations of O<sub>2</sub>, showing the inverse dependence of the observed rate constant on oxygen concentration.

**Table 3.** Activation Parameters for the Formation of Peroxo Species<sup>a</sup>

complex (solvent)	$\Delta H^\ddagger$ , kJ/mol	$\Delta S^\ddagger$ , J/mol·K
Fe(pydioneN <sub>5</sub> ) (DMF/CH <sub>3</sub> CN, 8:92 v/v)	38(2)	-134(30)
Fe(pydioneN <sub>5</sub> ) (DMF/CH <sub>3</sub> CN, 8:92 v/v, 50 equiv of 1-methylimidazole)	37(2)	-150(40)
Fe(pydioneN <sub>5</sub> ) (DMSO/CH <sub>3</sub> CN, 1:9 v/v)	61(2)	62(8)

<sup>a</sup> For determination of the activation parameters we used the value of  $k_{\text{obs}}[\text{O}_2]$  to build Eyring plots. In terms of elementary steps  $k_{\text{obs}}[\text{O}_2]$  represents  $k_2k_{-1}/k_1$ , see discussion in the main text.

First, the complex rapidly and reversibly (to account for the inverse oxygen dependence, vide infra) reacts with dioxygen to form an iron(III) superoxo species, which in turn reacts with another molecule of the starting iron(II) complex to produce a diiron peroxo intermediate.

The starting complex, Fe(pydioneN<sub>5</sub>), lacks the strong absorption band at ~450 nm, which is observed in the very

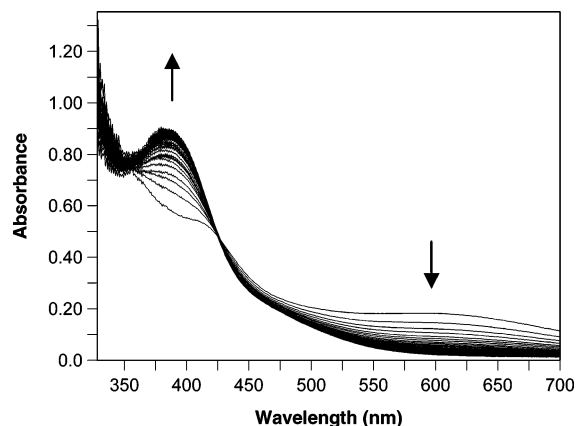


**Figure 13.** Spectral changes occurring during decomposition of the diiron peroxo intermediate in DMF/CH<sub>3</sub>CN 8:92 v/v at -10 °C over 200 s with strong UV irradiation of the sample, [Fe(pydioneN<sub>5</sub>)]<sub>0</sub> = 0.2 mM.

first spectra (ca. 20 ms after mixing the complex Fe(pydioneN<sub>5</sub>) with O<sub>2</sub>) and is attributed to the formation of the superoxo species on a time scale that is faster than can be observed by the stopped-flow method. The absorbance of this band decreases with the same rate constant as the corresponding increase in absorbance at ~650 nm (Figure 10), which is attributed to the formation of the peroxo-species. Therefore, we assign the band at 450 nm to an iron(III) superoxo species. Representative UV-vis spectra of the reaction at different times are shown in Figure 11.

The unusual inverse oxygen dependence (Figure 12), previously observed in the oxygenation of copper(I) complexes, can be explained by the following considerations.<sup>58</sup> The rate law for the rate-limiting step is described by the following equation:

$$\frac{d[(\text{LFe})_2\text{O}_2]}{dt} = k_2[\text{LFeO}_2][\text{LFe}] \quad (1)$$

The equilibrium binding of dioxygen to FeL is given by the following equation:

$$\frac{k_1}{k_{-1}} = K = \frac{[\text{LFeO}_2]}{[\text{LFe}][\text{O}_2]} \quad (2)$$

Substitution of (2) in (1) gives

$$\frac{d[(\text{LFe})_2\text{O}_2]}{dt} = k_2 \frac{[\text{LFeO}_2]^2}{K[\text{O}_2]} = k_{\text{obs}}[\text{LFeO}_2]^2 \quad (3)$$

i.e. the observed rate constant is as follows:

$$k_{\text{obs}} = \frac{k_2}{K[\text{O}_2]} = \frac{k_2k_{-1}}{k_1[\text{O}_2]} \quad (4)$$

We have also employed eq 4 in activation enthalpy and entropy analysis; for Eyring plots we took  $k_{\text{obs}}[\text{O}_2]$  to be equal to  $(k_2k_{-1})/k_1$ .

The decomposition of the peroxo species is much slower (ca. 2 orders of magnitude) than its formation (Figure 13).

(58) Zhang, C. X.; Kaderli, S.; Costas, M.; Kim, E.-I.; Neuhold, Y.-M.; Karlin, K. D.; Zuberhuhler, A. D. *Inorg. Chem.* **2003**, *42*, 1807–1824.

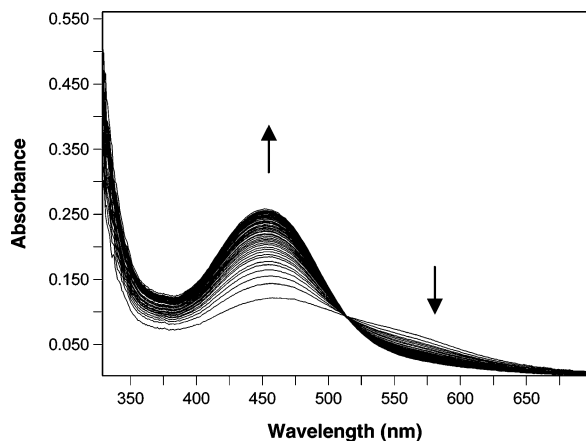


**Figure 14.** Time-resolved spectra acquired by the stopped-flow technique during the reaction of Fe(HpydioneN<sub>5</sub>)(Cl) (0.15 mM) with O<sub>2</sub> (4.1 mM) in DMSO/CH<sub>3</sub>CN 1:9 v/v at -40 °C over a 5 s time range.

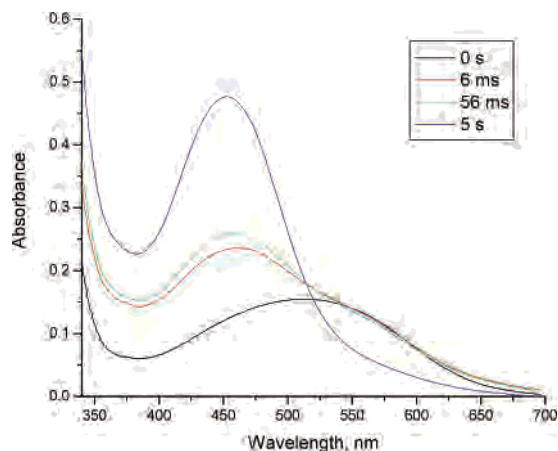


**Figure 15.** Overlay of UV-vis spectra of the reaction mixture at different times during the course of the reaction of Fe(HpydioneN<sub>5</sub>)(Cl) (0.3 mM) with O<sub>2</sub> (4.1 mM) obtained by the stopped-flow method at -40 °C in DMSO/CH<sub>3</sub>CN 1:9 v/v. Black line,  $t = 0$ , starting Fe(pydioneN<sub>5</sub>); red line,  $t = 0.006$  s, after mixing, the spectrum represents iron superoxo species; green line, 0.056 s; blue line, 5 s, the decomposition of superoxo species is essentially complete.

It should be noted that the peroxo intermediate is photosensitive; therefore, its decomposition studies were done in the single wavelength mode, thus minimizing light exposure of the sample. However, despite different rate constants, the spectral changes for the processes both with and without strong UV irradiation are the same (Figure 13).

Moreover, the stability of the peroxo intermediate can be enhanced by the addition of 1-methylimidazole or pyridine to the reaction mixture. For example, the oxygenation of Fe(pydioneN<sub>5</sub>) in DMF/CH<sub>3</sub>CN 8:92 v/v in the presence of ca. 50 equiv of 1-methylimidazole results in a  $t_{1/2}$  of >200 s for the peroxide decomposition at room-temperature! At the same time, 1-methylimidazole does not affect the activation parameters of peroxide formation. Even the addition of 500 equiv of 1-methylimidazole, instead of 50 equiv, results in identical (within experimental error) rate constants for the formation of the peroxo species in the same solvent system.

The decomposition of the peroxo intermediate formed by Fe(pydioneN<sub>5</sub>) in DMSO/CH<sub>3</sub>CN 1:9 v/v solvent mixture is first-order in the iron complex and zero-order in dioxygen. The activation parameters determined for this reaction are

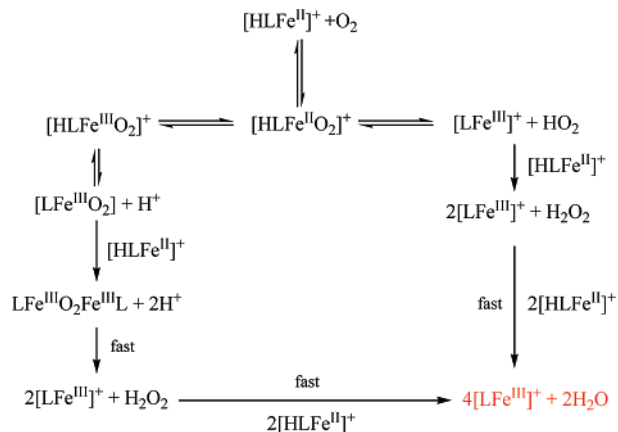
$\Delta H^\ddagger = 64(1)$  kJ/mol and  $\Delta S^\ddagger = -71(4)$  J/mol·K (Figure S10, Supporting Information). The final product of oxidation, the iron(III)  $\mu$ -oxo dimer, has also been characterized structurally with two molecules of 1-methylimidazole coordinated to both iron atoms (Figure 2).

Additional characterization of the observed intermediates is in progress with the goal of obtaining further structural information. EPR studies have shown that the peroxo intermediate is EPR silent, which is consistent with strong antiferromagnetic exchange normally observed in diiron(III) peroxides.

Oxygenation of the iron(II) complex with a monodeprotonated ligand, Fe(HpydioneN<sub>5</sub>)(Cl), in DMSO proceeds via a different pathway than the oxygenation of the dideprotonated complex.

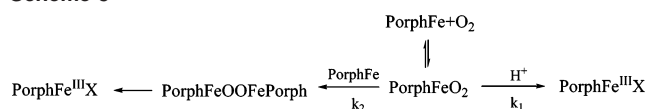
The absorbance changes observed during the oxygenation of Fe(HpydioneN<sub>5</sub>) are presented in Figure 14. The spectrum obtained immediately after mixing is fairly different from that of the initial iron(II) complex (Figure 15). The maximum at ~450 nm and a small increase in absorbance above 630 nm are reminiscent of the similar features observed upon formation of the superoxo species of Fe(pydioneN<sub>5</sub>). After these initial changes the absorbance continues to grow below 520 nm and decrease above 520 nm, with a tight isobestic point. The changes in the UV-vis spectrum are not as drastic as in the case of the dideprotonated complex because of the close overlap of the bands attributed to the superoxo species and the final iron(III) product. A double-exponential rate law is the best fit for the kinetic trace. The concentration dependence on [FeL] showed that both steps are first-order in iron(II). Under excess O<sub>2</sub>, the reaction is zero-order in dioxygen (Tables S12 and S13, Supporting Information). The UV-vis spectrum of the product of oxidation of the monodeprotonated complex is essentially identical to that of the iron(III) complex Fe(pydioneN<sub>5</sub>)(Cl) in DMSO, which suggests that it is the final product of oxygenation. These observations are consistent with the following two possible mechanisms (Scheme 4):

**Scheme 4.** Possible Mechanisms of Oxygenation of Fe(HPydioneN<sub>5</sub>)(Cl)



In accordance with the results obtained for the dideprotonated complex, the formation of the superoxo species from Fe(HpydioneN<sub>5</sub>) and O<sub>2</sub> is fast and is followed by the acid-

## Scheme 5



assisted decomposition of the intermediate. The importance of  $\text{H}^+$  in the oxygenation reaction can be illustrated by the fact that, in methanol, the reaction of  $\text{Fe}(\text{pydioneN}_5)$  with dioxygen proceeds in a similar fashion. The  $\text{pK}_a$  of the amide group is most likely lowered significantly due to stabilization of the conjugate base by the coordination to iron(III) in the resulting complexes.

The proton-assisted branching between different reaction pathways can be summarized as shown in Scheme 4. In all of the solvents, the iron(III) superoxo intermediate forms rapidly (within 0.02 s at  $-40^\circ\text{C}$ ). In protic solvents, or in the presence of an available proton from the amide group, there are at least two possibilities. In the first pathway, the superoxo species gets protonated, which is followed by the formation of non-coordinated  $\text{HO}_2$  and the iron(III) complex. Alternatively, in the second pathway, diiron(III) peroxide forms, and then  $\text{H}^+$  can rapidly react with this peroxo species. This possibility is less likely because of the observed first-order in  $[\text{FeL}]$ . In aprotic solvents or in the absence of available protons, the superoxo intermediate reacts with another molecule of the iron(II) complex to yield the diiron peroxo intermediate.

This behavior is identical to that of the iron(II) complexes with porphyrins, which are known to react with dioxygen via “binuclear” or “mononuclear” oxygenation pathways (Scheme 5).<sup>59</sup>

Moreover, the reaction pathways were drastically different for the oxygenation of iron(II) porphyrin complexes in the presence of different bases; 1-methylimidazole facilitated the reversible oxygenation of capped porphyrin complexes, whereas reactions with dioxygen in the presence of imidazole, added as the axial ligand, resulted in autoxidation.<sup>60,61</sup> These observations are consistent with the imidazole NH proton being responsible for promoting autoxidation. The  $\text{pK}_a$  of the imidazole NH proton is comparable to that of the amide NH proton, which makes this comparison especially valid. This proton-dependent behavior has also been observed in such processes as myoglobin autoxidation,<sup>62,63</sup> in the aerobic oxidation of non-porphyrin systems (2,2'-bi-2-imidazoline complexes of iron(II)),<sup>64</sup> as well as in the oxidation of simple iron(II) salts.<sup>65,66</sup> The two pathways shown in Scheme 4 are also consistent with the results of the mechanistic studies by van Eldik et al. of the EDTA–

$\text{Fe}(\text{II})$  system in aqueous solutions with careful pH control.<sup>67,68</sup> Such behavior is by no means unique to iron complexes and also has been observed for the oxygenation of cobalt(II).<sup>69</sup>

However, in the case of picket-fence, crowned, and hanging base porphyrins, where substituents on the porphyrin ring are linked by amide bonds, no proton-dependent behavior was observed.<sup>69,70</sup> The much slower rate of autoxidation in these complexes has been attributed to both the destabilizing of the charge separation associated with the formation of independent  $\text{Fe}(\text{III})$  and  $\text{O}_2^-$  and by limiting the accessibility of water inside hydrophobic pockets.<sup>71,72</sup>

It should also be noted that Kimura et al. observed the formation of the intermediate assigned as a peroxo species during the oxygenation of an iron(II) complex with a very closely related pyridine-containing pentaaza macrocyclic ligand in an aqueous solution.<sup>73</sup> The rate of formation of this remarkably stable reported species is much slower ( $1.4(2) \times 10^2 \text{ M}^{-1}\cdot\text{s}^{-1}$  at pH 8.0), even at room-temperature, compared to the oxygenation of its amide counterpart  $\text{Fe}(\text{pydioneN}_5)$ , which occurs at room-temperature faster than it can be observed by the stopped-flow technique ( $k_{\text{obs}}$  as extrapolated from activation parameters is  $2 \times 10^7 \text{ M}^{-1}\cdot\text{s}^{-1}$ ). The reported<sup>73</sup> extinction coefficient of the band at 540 nm ( $187 \text{ M}^{-1}\cdot\text{cm}^{-1}$ ) is also relatively small when compared to the values for other diiron peroxo species. The presence of deprotonated amide groups in the ligand **1** greatly facilitates the reactions of iron(II) complexes with dioxygen.

## Conclusions

We have prepared iron(II) complexes of the pentadentate amide-containing macrocycles **1** and **1a**. Interestingly, we have obtained both mono- and dideprotonated versions of the iron(II) complex. The deprotonation state is maintained in the DMSO solution. The rigid nature of the macrocycle enforces a pentagonal–bipyramidal geometry, which precludes the low-spin state in the  $d^6$  system. It also limits the range of the iron–donor atom distances which, when coupled with the large size of the ring, causes all iron(II) complexes (including pseudo-octahedral  $\text{Fe}(\text{HpydioneN}_5)(\text{Cl})$ ) to be high-spin, even at low-temperature.

We have studied the oxygenation reactions of these complexes in detail, both spectroscopically and kinetically. The deprotonation state of the complex has a profound effect on its reactivity with dioxygen. Oxygenation of the dideprotonated complex of  $\text{Fe}(\text{II})$ ,  $\text{FePydioneN}_5$ , in aprotic solvents proceeds via the analogous path to that of iron(II) porphyrins: via iron(III) superoxo and diiron(III) peroxo species.

(59) Brinigar, W. S.; Chang, C. K.; Geibel, J.; Traylor, T. G. *J. Am. Chem. Soc.* **1974**, *96*, 5597–5599.

(60) Almog, J.; Baldwin, J. E.; Huff, J. *J. Am. Chem. Soc.* **1975**, *97*, 227–228.

(61) Almog, J.; Baldwin, J. E.; Dyer, R. L.; Huff, J.; Wilkerson, C. J. *J. Am. Chem. Soc.* **1974**, *96*, 5600–5601.

(62) Shikama, K. *Coord. Chem. Rev.* **1988**, *83*, 73–91.

(63) Shikama, K. *Chem. Rev.* **1998**, *98*, 1357–1373.

(64) Burnett, M. G.; McKee, V.; Nelson, S. M. *J. Chem. Soc., Chem. Commun.* **1980**, 599–601.

(65) George, P. *J. Chem. Soc.* **1954**, 4349–4359.

(66) Hammond, G. S.; Wu, C.-H. *Adv. Chem. Ser.* **1968**, *77*, 73.

(67) Seibig, S.; van Eldik, R. *Inorg. Chem.* **1997**, *36*, 4115–4120.

(68) Zang, V.; van Eldik, R. *Inorg. Chem.* **1990**, *29*, 1705–1711.

(69) Warburton, P. R.; Busch, D. H., In *Perspectives in Bioinorganic Chemistry*; Hay, R. W.; Dilworth, J. A.; Nolan, K. B., Eds.; JAI Press: London, 1993; Vol. 2, pp 1–93.

(70) Momenteau, M.; Reed, C. A. *Chem. Rev.* **1994**, *94*, 659–698.

(71) Wang, J. H.; Nakahara, A.; Fleischer, E. B. *J. Am. Chem. Soc.* **1958**, *80*, 1109–1113.

(72) Kitahara, Y.; Matsuoka, A.; Kobayashi, N.; Shikama, K. *Biochim. Biophys. Acta* **1990**, *1038*, 23–28.

(73) Kimura, E.; Kodama, M.; Machida, R.; Ishizu, K. *Inorg. Chem.* **1982**, *21*, 595–602.

### *Iron(II) Complexes with Amide-Containing Macrocycles*

This is evidenced by the spectral changes during the reaction, a second-order dependence in iron(II) complex concentration, and an inverse dependence of the reaction rate on the dioxygen concentration. The final product of oxygenation is a crystallographically characterized iron(III)  $\mu$ -oxo dimer. We have also found that the presence of 1-methylimidazole can stabilize the diiron peroxo intermediate, and the half-life of the intermediate increases by ca. 2 orders of magnitude in a large excess of 1-methylimidazole.

The reaction of Fe(pydioneN<sub>5</sub>) with dioxygen is distinctly different in methanol. The reaction is first-order in both iron(II) complex and dioxygen, and no intermediate is spectroscopically observed. A similar behavior was observed for the monodeprotonated complex, Fe(HpydioneN<sub>5</sub>). The presence of an accessible proton in the vicinity of the reaction center (originating either from the solvent or from the amide group of the ligand) proves to be sufficient to alter the oxygenation pathway in these macrocyclic systems, which is similar to the properties of iron(II) porphyrin complexes. The new amidopyridine macrocycles can be considered new members of the "expanded porphyrin analogue" family. The expansion of the cavity provides control over the spin state

and the availability of protons. These macrocyclic systems also allow for easy synthetic modifications, thereby paving the way to new, versatile metal complexes.

**Acknowledgment.** This research was supported by the U.S. Department of Energy-Office of Basic Energy Sciences, Grant No. DE-FG02-06ER15799. The EPR facility at Tufts is supported by the NSF (CHE 9816557). The CCD based X-ray diffractometer at Tufts University was purchased through Air Force DURIP Grant F49620-01-1-0242. The CCD based X-ray diffractometer at Harvard University was purchased through NIH Grant No. 1S10RR11937-01. The NMR facility in the Chemistry Department at Tufts University is supported by NSF Grant No. CHE-9723772. AC susceptometry and DC/AC SQUID magnetometry instrumentation at Northeastern University were purchased through the partial support of NSF instrumentation grants.

**Supporting Information Available:** X-ray crystallographic files in CIF format as well as additional figures and tables summarizing spectroscopic and kinetic data. This material is available free of charge via the Internet at <http://pubs.acs.org>.

IC0701209